Mineralogical Magazine, October 2007, Vol. 71(5), pp. 553–569

The crystal structures, solid solutions and infrared spectra of copiapite-group minerals

J. MAJZLAN* AND R. MICHALLIK

Institute of Mineralogy and Geochemistry, Albert-Ludwig University of Freiburg, Albertstraße 23b, D-79104 Freiburg, Germany

[*Received 13 September 2007; Accepted 18 March 2008*]

ABSTRACT

Copiapite is a mineral of iron- and sulphate-rich acidic environments and has a general formula $A Fe_4^{3+}(SO_4)_6(OH)_2(H_2O)_{20}$, where A = Fe^{2+}, $2/3Fe^{3+}$, $2/3Al^{3+}$, Mg, Zn. The structure is built by infinite tetrahedral-octahedral chains and isolated octahedrally coordinated A sites. Our synthetic and natural copiapite samples can be divided into two large groups based on the orientation of the structural fragments. One group comprises copiapite phases where A = Al^{3+}, Fe^{2+} or Fe^{3+} and we designate it as the structural type AL. The other group consists of copiapite with A = Mg^{2+}, Zn^{2+} or Ni^{2+} and this is the structural type MG. The solid-solution series between Fe^{3+} and Al^{3+} copiapite is continuous. The series between Mg^{2+}-Al^{3+}, Mg^{2+}-Fe^{3+} and Mg^{2+}-Al^{3+}-Fe^{3+} copiapite are not continuous; the samples with intermediate compositions contain two copiapite phases, one of the type AL and one of the type MG. The series between Mg^{2+} and Zn^{2+} copiapite is continuous only at 25ºC. At 75ºC, the Zn-rich portion of this system crystallizes a copiapite-like phase whose structure may be a superstructure of copiapite. The series between Al-Fe^{2+} and Mg-Fe^{2+} copiapite are not continuous and show complex behaviour of the intermediate compositions.

KEYWORDS: copiapite, crystal structures, solid solutions, infrared spectra.

Introduction

COPIAPITE was first described from Copiapo (Chile) by Rose (1833) as *basisches schwefelsaures Eisenoxyd*. Interestingly, the original sample analysed by Rose (1833) belongs to magnesiocopiapite, although the name copiapite was assigned later to a mineral with composition $Fe^{2+}Fe_4^{3+}(SO_4)_6(OH)_2(H_2O)_{20}$ by Haidinger (1845). Rammelsberg (1860) listed several analyses of copiapite and related materials and gave their formulae. Based on its crystal morphology, copiapite was assigned to the orthorhombic or monoclinic crystal class (see discussion in Scharizer, 1913). Scharizer (1913) also distinguished copiapite with the components Fe_2O_3, H_2SO_4 and H_2O (today called ferricopiapite) and copiapite containing additional components. Since then, this mineral has been found at many localities where sulphidic minerals weather and release Fe(II), Fe(III), other cations and $(SO_4)^{2-}$ into aqueous solutions (e.g. Jamieson *et al*., 2005). The synthesis of copiapite has been reported by Walter-Levy and Quemeneur (1963), Atencio *et al*. (1996), Broemme and Poellmann (2007) and Friedlander *et al*. (2007). The crystal structure of copiapite has been solved by Süsse (1972) and Fanfani *et al*. (1973). Despite these two works, the details of the crystal structure and crystal chemistry of this group of minerals remain poorly known. Bayliss and Atencio (1985) list lattice parameters of several copiapite samples refined by least-squares methods.

In this work, we have analysed the crystal structure of a number of copiapite samples by powder X-ray diffraction (XRD) (both in-house and synchrotron). The studied samples include both synthetic and natural material. We explored

* E-mail: Juraj.Majzlan@minpet.uni-freiburg.de
DOI: 10.1180/minmag.2007.071.5.553

the subtle variations in the structure of copiapite and their impact on the XRD patterns. Such variations affect the miscibility of the end-members; the solid solutions among the end-members have been assumed to be continuous until now. We have also collected infrared (IR) spectra of selected copiapite samples.

Materials and methods

Natural samples used in this study were acquired from mineral dealers and details of their formation conditions are unknown. The parts of the samples believed to be copiapite were separated under a binocular microscope. The separate was then ground gently and stored in double-walled vials to minimize the interaction of the powdered samples with the ambient atmosphere. We found that the samples tend to decompose to a reddish phase in our laboratory where the relative humidity varies between 30 and 40%.

The chemicals used for the syntheses were: deionized water (conductivity 0.055 μS/cm); ferric sulphate, a fine-grained, hygroscopic chemical with an approximate composition $Fe_2(SO_4)_3 \cdot 6.25H_2O$; and metal sulphates (i.e. sulphates of metals other than Fe^{3+}) $MgSO_4 \cdot 7H_2O$, $Al_2(SO_4)_3 \cdot 17H_2O$, $FeSO_4 \cdot 7H_2O$, $ZnSO_4 \cdot 7H_2O$, $NiSO_4 \cdot 7H_2O$ and $CuSO_4 \cdot 5H_2O$ (all solid chemicals p.a.). All solid chemicals were used as received, i.e. no variations from the nominal hydration state were taken into account. The amount of chemicals used for the syntheses of the end-members is listed in Table 1. The amounts used for the syntheses of the intermediate compositions are available as supplementary information to this publication, and can be found at http://www.minersoc.org/pages/e_journals/dep_mat.html. For the binary series between the end-members X and Y, the amounts were calculated at X/(X+Y) intervals of 0.1. In the Mg-Fe^{3+}-Al ternary system, the initial compositions were prepared at regular Al/(Mg+Fe^{3+}+Al), Mg/(Mg+Fe^{3+}+Al), or Fe^{3+}/(Mg+Fe^{3+}+Al) increments of 0.1 in order to cover the entire compositional space. For samples which did not contain Fe^{2+}, polyethylene vials with a total volume of 15 ml were first filled with water and a metal sulphate. This mixture was shaken until the metal sulphate dissolved completely. For samples with Fe^{2+}, water and the ferrous sulphate were mixed and stirred in a small beaker until the solid dissolved completely. This procedure was necessary because the ferrous sulphate was dissolving very slowly in the polyethylene vials and the product in these cases was a mixture of melanterite and Fe^{2+}-depleted copiapite. Afterwards, ferric sulphate was added and quickly dissolved. The vials were closed tightly and the viscous brown liquid was then maintained at the desired temperature (25ºC, 75ºC, 110ºC) until voluminous precipitate formed. The mass was washed repeatedly with ethanol, separated from the mixture of ethanol and remaining interstitial liquid by filtration, and dried at room temperature.

The XRD patterns of the natural samples were collected at the bending magnet beamline DIFF at the synchrotron light source ANKA (Angströmquelle Karlsruhe, Germany) or the beamline X16C at the National Synchrotron Light Source (Brookhaven National Laboratory, USA). The synchrotron was used because of the small amount of material available and contamination of several natural samples by other phases. X-rays of wavelengths 0.71874(1) Å (ANKA) or

TABLE 1. Starting compositions for end-member synthesis. Note that not all samples formed the phase intended to precipitate; see text for details.

Sample	Water (ml)	Ferric sulphate (g)	Sulphate of metal other than Fe^{3+} (g)	Intended to precipitate
HSC-1	1.20	2.0221	$MgSO_4 \cdot 7H_2O$ 0.4779	Magnesiocopiapite
HSC-11	1.20	2.5000	–	Ferricopiapite
HSC-21	1.20	2.0709	$Al_2(SO_4)_3 \cdot 17H_2O$ 0.4291	Aluminocopiapite
HSC-95	1.20	1.9597	$ZnSO_4 \cdot 7H_2O$ 0.5403	Zincocopiapite
HSC-96	1.20	1.9696	$NiSO_4 \cdot 7H_2O$ 0.5304	Ni analogue of copiapite
HSC-128	1.20	1.9738	$FeSO_4 \cdot 7H_2O$ 0.5262	Copiapite
HSC-150	1.20	2.0980	$CuSO_4 \cdot 5H_2O$ 0.2490	Cuprocopiapite

0.69244(1) Å (NSLS) were selected by a double crystal Si(111) monochromator. The wavelength and the zero angle of the diffractometer were determined with silicon powder (NIST standard reference material 640). The sample was loaded into a 1.0 mm glass capillary which was rotated about its axis during data collection. The intensity of the incoming beam was monitored during the data collection by an ion chamber and the measured intensities of the diffracted beam were corrected for the decay and fluctuations of the primary beam. The XRD patterns were collected at room temperature, over an angular range of 1.8–33.8º2θ, with step of 0.008º2θ and counting time of 2 s per point.

The powder XRD patterns of the synthetic samples were collected with a Bruker AXS D8 Advance diffractometer, using Cu-*K*α radiation, a diffracted-beam graphite monochromator, and a scintillation detector. The samples were front-loaded into plastic holders which spun during the data collection. The XRD patterns were collected from 5–60º2θ with a step of 0.02º2θ and dwell of 3 s. Most samples were used as synthesized; some demonstrated strong preferred orientation and were gently ground prior to the XRD analysis.

All diffraction experiments were performed at room temperature. The structural models, applied to the collected patterns, were refined using Rietveld refinement with the program GSAS (Larson and von Dreele, 1994). The starting models were the structures reported by Süsse (1972), Fanfani *et al*. (1973) and Majzlan and Kiefer (2006). Starting models for paracoquimbite and pickeringite (impurities in the natural samples) were taken from Robinson and Fang (1971) and Quartieri *et al*. (2000), respectively. The following parameters were allowed to vary during the refinement: lattice parameters, Gaussian and Lorentzian broadening of the peak profiles (parameters GP and LX in GSAS), vertical displacement of the specimen (parameter shift in GSAS) and the phase fraction, if more than one phase was present. The composition at the *A* site of each copiapite sample was set to that determined by chemical analysis and not refined further.

Single-crystal XRD experiments on one selected sample were carried out at the undulator XRD beamline X06SA at the Swiss Light Source (Paul Scherrer Institute, Villigen, Switzerland). This experiment was performed on one sample only because the powder data for this sample could not be indexed as copiapite. A $10 \times 10 \times 1$ μm large crystal was attached to a microloop using commercial silicon grease. The crystal was inserted into a beam (25×5 μm) in the micro-crystal diffractometer. The wavelength $\lambda = 0.7246$ Å of the X-ray beam was selected using a Si(111) monochromator. The diffraction pattern was collected using a mar225 mosaic CCD detector and indexed using X-ray dispersive spectroscopy (XDS) software.

The Fourier transform infrared (FTIR) spectra of selected samples were collected using a Bruker Equinox 55 FTIR spectrometer with a Globar source and a liquid N_2-cooled MCT detector. The samples were embedded in a KCl pellet (200 mg KCl and 2 mg of sample) and analysed in transmission mode. Although KBr is commonly used for this purpose, we found that the samples reacted with and decomposed in contact with KBr. A spectrum of a KCl pellet devoid of any copiapite sample was collected prior to each copiapite sample spectrum and used as a background. The optics of the spectrometer and the sample chamber were evacuated during the data collection.

The concentration of the cations in the samples was determined with an Analytik Jena Vario 6 atomic absorption spectrometer (AAS). The samples were dissolved in deionized water and an appropriate amount of concentrated distilled HCl and 30% CsCl solution was added. The samples were analysed for Fe, Al, Mg, Zn, Ni and Cu, as needed.

The concentration of Fe^{2+} in selected samples was measured by dissolving the sample in 50 ml of water, adding 5 ml of ammonium acetate buffer (prepared by mixing 40 g of $(NH_4)CH_3COO$, 50 ml of glacial acetic acid and adding water to a total volume of 100 ml), 2 ml of phenantroline solution (0.5 g of $C_{12}H_9ClN_2 \cdot H_2O$ dissolved in water and adjusting the volume to 100 ml), and measuring the absorbance of the solution at 510 nm with a Perkin-Elmer Lambda 40 UV/vis spectrometer. The concentration of Fe^{3+} was calculated as the difference between total Fe and Fe^{2+}. The water content of the copiapite samples was assumed to be equal to the nominal value.

Composition and structure of copiapite

The term copiapite is not only the name of a triclinic mineral with the formula $Fe^{2+}Fe^{3+}_4(SO_4)_6(OH)_2(H_2O)_{20}$ but also the name of a group of structurally and chemically related minerals with the general formula

$A Fe_4^{3+}(SO_4)_6(OH)_2(H_2O)_{20}$, where A = Fe^{2+}, $2/3Fe^{3+}$, 2/3Al, Mg, Zn or Cu. These minerals were assumed to be isostructural despite the differences in the structural models for ferricopiapite (Fanfani *et al*., 1973) and magnesiocopiapite (Süsse, 1972). Fanfani *et al.* (1973) commented on these differences but no other work has been carried out to resolve this problem.

The description of the structure of copiapite was completed by Majzlan and Kiefer (2006) who employed powder neutron, XRD and *ab initio* calculations. They located the hydrogen atoms in this complicated strucure and found that the structure can be described as a combination of infinite chains $[Fe_4(SO_4)_6(H_2O)_8(OH)_2](H_2O)_2$ and slabs of composition $\{[A(H_2O)_6](H_2O)_4\}$ (Fig. 1). The A site is coordinated octahedrally and is isolated from the infinite chains, i.e. only connected to the chains via a network of hydrogen bonds. If the A site is occupied by Fe^{3+} or Al^{3+}, the condition of electrostatic neutrality requires one third of the A sites to be vacant. The presence of these vacancies may cause a re-arrangement of the hydrogen bond network (Majzlan and Kiefer, 2006).

Results

Within the resolution of the powder XRD experiments, the copiapite samples synthesized in this study did not contain other phases. The only exception was the Mg-Fe^{3+} solid-solution series, contaminated by kornelite. Other authors (e.g. Friedlander *et al*., 2007) reported that rhomboclase is a common by-product of copiapite synthesis. However, they synthesized their samples by mixing solid sulphates with sulphuric acid and allowing partial evaporation of the solutions at elevated temperatures. The size of the stability fields of most copiapite minerals as a function of solution compositions is not known, but the stability field of ferricopiapite is very narrow (see Posnjak and Merwin, 1922). Hence, evaporation or even small variations in the sample preparation protocol (i.e. different amounts of H_2SO_4 added) could easily lead to a shift of the system into the stability field of another Fe sulphate, e.g. rhomboclase. In our work, no sulphuric acid was used, and the samples were not allowed to evaporate. If the vials were found to leak, the runs were discarded and the syntheses repeated. Therefore, if pure samples are sought,

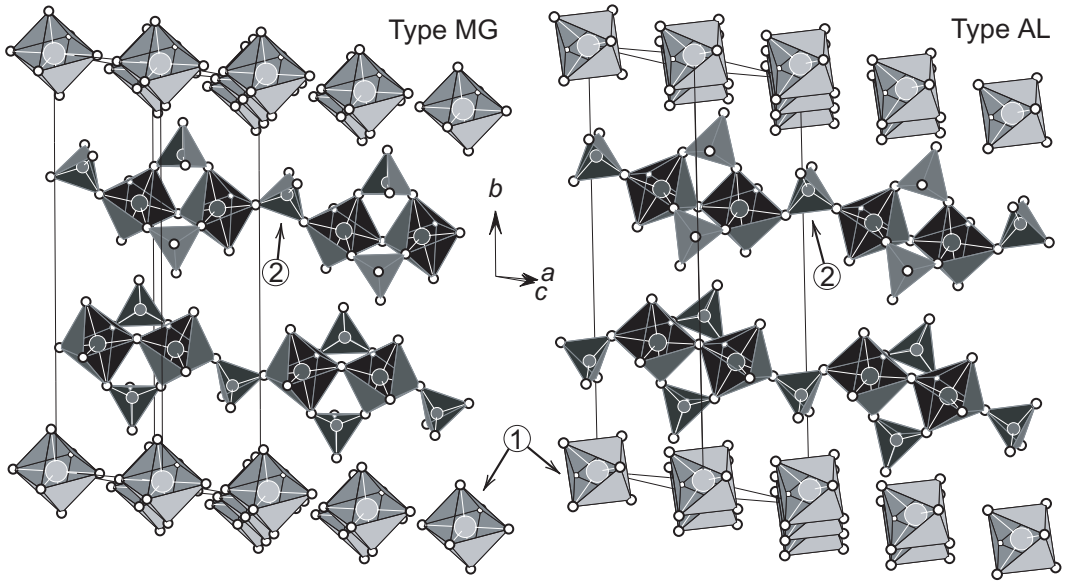

FIG. 1. Fragments of the structure of magnesiocopiapite (structural type MG) and ferricopiapite (structural type AL) projected onto $\bar{1}01$. The isolated octahedra that house the A cations are shown as light grey, the infinite chains as dark grey. The main differences between the two structural types are in the orientation of the isolated octahedra (marked by arrows labelled 1) and the orientation of the sulphate tetrahedra within the infinite chains (marked by arrows labelled 2).

we consider our synthetic procedure superior to those of others.

The copiapite samples investigated in this study can be divided into two groups based on their structural features (Table 2). The principal differences lie in the orientation of the isolated $A(H_2O)_6$ octahedra and the topology of the infinite chains (Fig. 1). When the *A* site is occupied by cations Mg^{2+}, Ni^{2+} or Zn^{2+}, the structures can be refined with the magnesiocopiapite model of Süsse (1972). We will label this structural type as the type MG. If the *A* site houses the cations Al^{3+}, Fe^{3+} or Fe^{2+}, the structures can be refined with the ferricopiapite model of Fanfani *et al*. (1973). This is the structural type AL. The unit-cell volume of the type MG copiapite is larger than that of type AL copiapite (Table 2). The trivalent ions form copiapite of the type AL; all divalent ions apart from Fe^{2+} form copiapite of the type MG. The copiapite with Fe^{2+} belongs to the type AL but its unit-cell volume is intermediate between that of type MG copiapite and the copiapite samples with Fe^{3+} and Al^{3+}. The reason for this anomalous behaviour of Fe^{2+} within the copiapite-group of minerals is unclear.

Although the structural differences are subtle, they lead to clear variations in the peak intensities of powder XRD patterns (Fig. 2). These variations can be used to determine the structural type of a studied copiapite sample. It should be emphasized that a successful determination of the structural type for a copiapite sample assumes that the systematic errors that contribute to the intensity of the XRD peaks have been suppressed to a minimum. In particular, preferred orientation is a significant problem when collecting XRD patterns of the copiapite minerals which tend to form platy crystals.

Because of the relatively large number of copiapite samples synthesized in this study, their composition, number of phases and lattice parameters cannot be all listed in this publication. The data for all our samples (composition of the initial solution, composition of the final product, number of phases, lattice parameters) are available as supplementary information and can be downloaded from the Mineralogical Society website at http://www.minersoc.org/pages/e_journals/dep_mat.html.

In addition to the two structural types of the copiapite-group minerals, another phase closely related to copiapite has been identified in our study. This phase was synthesized in the systems that contain Zn or Ni at $T = 75$ºC and is described in the respective sections below. Initially, we considered this phase to be a member of the

TABLE 2. Lattice parameters of the end-members synthesized in this study. The values in parentheses are the estimated standard deviations. The column-type describes the structure of the phase: structural type MG, AL or a copiapite-like (CL) phase. Column *A* specifies the composition at the *A* site. The lattice parameters *a*, *b*, *c* are in Å; α, β, γ are in degrees.

Sample	*A*	Type	*a*	*b*	*c*	α	β	γ	*V*
Synthesized at $T = 25$ºC									
HSC-1	Mg	MG	7.3451(4)	18.794(1)	7.3891(4)	91.369(5)	102.169(4)	98.831(4)	983.6(1)
HSC-11	Fe^{3+}	AL	7.3871(5)	18.362(1)	7.3286(4)	93.938(5)	102.208(4)	98.920(4)	954.5(1)
HSC-21	Al	AL	7.3853(7)	18.249(2)	7.3280(6)	93.873(7)	102.221(6)	99.163(6)	947.7(2)
HSC-95	Zn	MG	7.359(18)	18.69(5)	7.417(15)	91.03(14)	102.25(14)	98.19(15)	985.4(41)
HSC-96	Ni	MG	7.411(19)	18.63(6)	7.467(17)	92.30(14)	102.47(13)	96.72(16)	997.7(46)
HSC-128	Fe^{2+}	AL	7.3858(9)	18.592(3)	7.3543(8)	92.273(9)	102.274(8)	98.290(9)	973.9(2)
Synthesized at $T = 75$ºC									
HSC-147	Mg	MG	7.3468(5)	18.794(1)	7.3874(5)	91.365(6)	102.184(5)	98.820(5)	983.6(1)
HSC-148	Fe^{3+}	AL	7.3873(2)	18.356(1)	7.3280(2)	93.963(2)	102.202(2)	98.939(2)	954.1(1)
HSC-149	Al	AL	7.3838(4)	18.249(1)	7.3243(4)	93.902(4)	102.198(4)	99.171(4)	947.0(1)
HSC-79	Zn	CL	7.3501(4)	36.382(2)	7.3326(4)	93.184(3)	102.176(4)	92.458(3)	1910.7(2)
HSC-151	Ni	CL	7.3504(3)	36.311(2)	7.3354(3)	93.187(3)	102.152(3)	92.498(3)	1907.9(1)
Synthesized at $T = 110$ºC									
HSC-90	Mg	MG	7.345(3)	18.786(7)	7.389(3)	91.41(3)	102.15(3)	98.80(3)	983.4(7)
HSC-94	Al	AL	7.390(4)	18.302(12)	7.324(4)	93.91(5)	102.26(4)	98.93(5)	951.1(9)

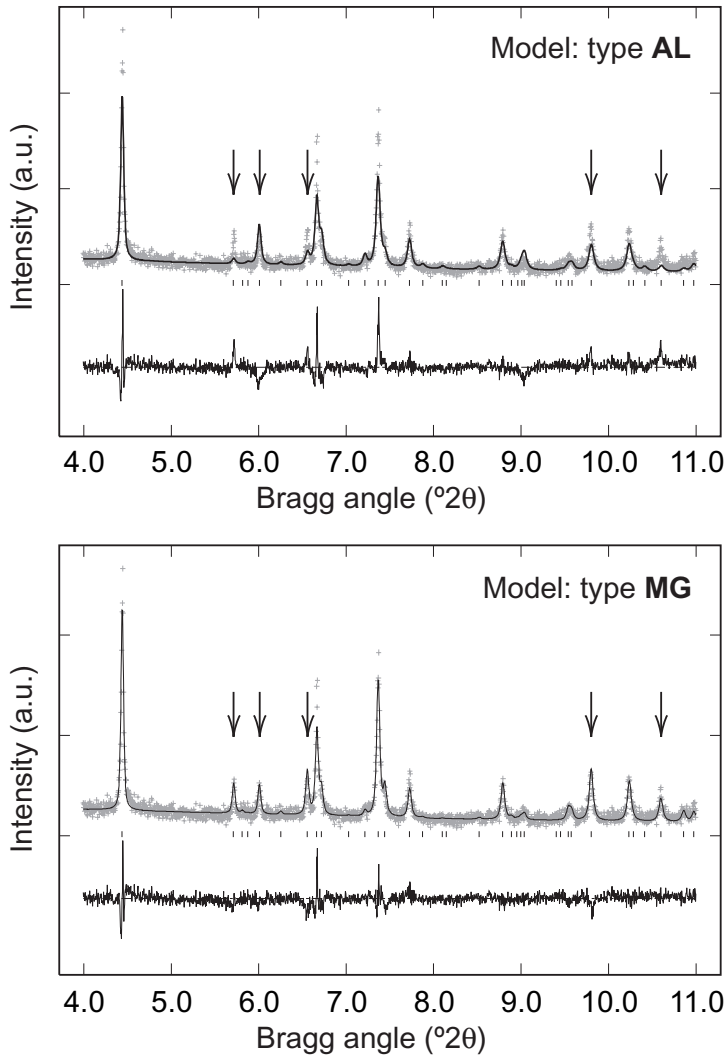

FIG. 2. Result of the Rietveld refinement for a natural Zn-Mg copiapite sample (see Table 5 for its lattice parameters) using a model with structural types AL (upper) and MG (lower). This sample belongs to the structural type MG. The arrows show the regions with the largest differences between the two refinements. The crosses are the measured data, the curve fitting them was calculated from the model. The curve below the pattern is the difference curve.

copiapite group due to the striking similarity of the crystal habit, solubility in water, XRD pattern and FTIR spectra. However, closer scrutiny of the XRD data revealed that the patterns cannot be indexed with the unit cell of copiapite. The attempts to index the powder data invariably failed. Afterwards, we were able to obtain a single-crystal XRD pattern from a single platelet 10 μm wide and ~1 μm thick. Instrumental difficulties and the small size of the crystal precluded the collection of a complete set of intensities. However, the data were of sufficient quality to suggest several possible unit cells. The cell with a = 7.3501(4) Å, b = 36.382(2) Å, c = 7.3326(4) Å, α = 93.184(3)º, β = 102.176(4)º, γ = 92.458(3)º fit the powder XRD pattern to a LeBail χ^2 = 2.3. It should be noted that all cell parameters with the exception of b are very similar to those of the cell for copiapite; the value of b for this phase is double that of copiapite. Therefore, the

structure of this copiapite-like phase appears to be a derivative or a superstructure of the copiapite structure. We will attempt to solve the structure from the powder data and, if successful, the results will be reported elsewhere.

End-members synthesized at 25°C

All solutions prepared at 25ºC precipitated a crystalline phase within 24–48 h. Almost the entire volume of the starting viscous liquid was converted into a thick yellow paste of minute copiapite crystals (1–2 μm). The copiapite phases with *A* cations Mg^{2+}, Al^{3+}, Fe^{3+} and Fe^{2+} represent well crystallized phases (Table 2). The phases with *A* cations Zn^{2+} and Ni^{2+} were of significantly poorer crystallinity. The Gaussian and Lorentzian broadening of the peaks of the Zn- and Ni-copiapite was much greater than that of the other copiapite samples. In addition, the fit statistics for the Zn- and Ni-copiapite were considerably worse. These facts indicate that the incorporation of Zn^{2+} and Ni^{2+} into the structure of copiapite is not as favourable as the incorporation of Mg^{2+}, Al^{3+}, Fe^{3+} or Fe^{2+}. The copiapite samples with $A = Mg^{2+}$, Zn^{2+} and Ni^{2+} belong to the structural type MG, while those with $A = Al^{3+}$, Fe^{3+} and Fe^{2+} belong to the structural type AL.

The sample prepared to precipitate Cu-copiapite formed a phase unrelated to copiapite. The product of this synthesis consists of small (20–30 μm) prismatic crystals pale-green in colour. Indexing with the program ITO (Visser, 1969) suggested a B-centred cell with a figure-of-merit (FOM) of 98.1 and all 20 of the first 20 lines indexed. Subsequent LeBail refinement with GSAS led to a LeBail χ^2 of 2.5 and confirmed that the cell with a = 11.6718(5) Å, b = 11.5543(5) Å, c = 6.1278(3) Å, α = 87.086(3)º, β = 102.661(3)º and γ = 115.227(2)º can satisfactorily describe the observed data. To our knowledge, the crystal structure of this phase has not been solved and reported yet.

End-members synthesized at 75°C

The samples maintained at 75ºC precipitated 7–40 days after the starting solutions were prepared. The products were coarser than the material prepared at 25ºC. The crystals have a platy habit and reach sizes of up to 50 μm. However, the larger crystals are always intergrown with smaller ones and not suitable for single-crystal diffraction experiments. Single crystals potentially useable for such experiments are those <10–15 μm. The strong 0*k*0 preferred orientation observed in the XRD patterns proves that the dominant form of our copiapite crystals is the pinacoid {010}. Although the crystal size of the samples prepared at 75ºC is significantly larger than that for the 25ºC samples, the peak broadening is comparable for both sets of the end-member copiapite phases.

At T = 75ºC, only the syntheses with Mg^{2+}, Al^{3+}, Fe^{3+} and Cu^{2+} yielded a copiapite phase (Table 2). The copiapite phase with Mg^{2+} belongs to the structural type MG, those with Al^{3+} and Fe^{3+} to the structural type AL, as expected. The Cu-copiapite sample was considerably more disordered than the Mg-, Al- and Fe^{3+}-copiapite prepared at 75ºC. Yet, it was possible to obtain a satisfactory fit to the XRD data. The chemical analysis suggests that this sample was not an end-member but the composition at the *A* site was $Cu_{0.40}Fe_{0.39}$. Therefore, our sample is an intermediate phase of the cuprocopiapite – ferricopiapite series with unit-cell volume of 953.7(2) $Å^3$ and belongs to the structural type AL.

Multiple syntheses with Fe^{2+} failed to produce a well-crystalline copiapite phase. These runs yielded disordered, probably fully oxidized material. The syntheses with Zn^{2+} and Ni^{2+} produced a copiapite-like phase (Table 2). We have also attempted to prepare calciocopiapite, either by mixing gypsum or calcium chloride with the ferric sulphate solution. In both cases, gypsum was the only product identified in the solid collected at the end of the synthesis.

End-members synthesized at 110°C

In the solutions maintained at 110ºC, precipitate appeared after 3–6 days. All samples synthesized at 110ºC contained $Fe(OH)SO_4$ as the dominant phase. From all the end-member compositions prepared, only the syntheses with Mg^{2+} and Al^{3+} yielded a copiapite phase (Table 2). The phase $Fe(OH)SO_4$ was previously reported at elevated temperatures ($\geqslant$110ºC) in the system Fe_2O_3-SO_3-H_2O by Posnjak and Merwin (1922) and its structure was solved by Johansson (1962). This structural model was used in the Rietveld refinement to confirm the presence of $Fe(OH)SO_4$. The temperature of 110ºC appears to be close to the uppermost limit at which copiapite can crystallize or persist under ambient-pressure conditions.

The $Fe^{3+}-Al$ join at 25°C and 75°C

The entire series between the $Fe^{3+}-Al^{3+}$ copiapite end-members was synthesized at T = 25ºC and 75ºC (Table 3, Fig. 3*a*). The synthesized samples show no clear preference for uptake of Fe^{3+} or Al^{3+} from the solution, i.e. the composition of the solid copiapite samples is close to the composition of the initial solution (Fig. 3*a*). Both end-members belong to the structural type AL and therefore the solid solution could be continuous, although the large cation size difference between Fe^{3+} and Al^{3+} (20%) may cause immiscibility in this system. Since the lattice parameters of the end-members are similar, the presence of two phases in the intermediate samples could be detected only if the peak-broadening parameters in the solid solution members were systematically larger than those for the end-members. We have carefully compared the refined values of the Gaussian and Lorentzian broadening and found no evidence for the existence of two copiapite phases in our samples. Hence, each copiapite sample along the $Fe^{3+}-Al^{3+}$ join consists of a single phase of the type AL.

The unit-cell volume (V) shows negative deviation from the ideal mixing line (Fig. 3*a*). The deviation is only slight among the samples prepared at 25ºC, but distinct in the samples produced at 75ºC. Among the lattice parameters, the greatest changes are observed in the parameter b, with the variation in V essentially mimicking the variations of b. The lattice parameters a, c, α, β and γ vary within relatively narrow bounds, with α increasing and γ decreasing throughout the series from the Fe^{3+} to the Al^{3+} end-member.

The Mg−Al join at 25°C and 75°C

The structures of the two end-members in this series belong to two different structural types. As a result, the solid solution is not expected to be continuous. Indeed, the intermediate compositions crystallized two phases at T = 75ºC, one with the type AL structure and another with the type MG structure (Table 4, Fig. 3*b*). The two phases are clearly distinguished by their XRD patterns because the significant difference in the lattice parameter b causes a clear separation of their 020 peaks (Fig. 4*a*). The systems more abundant in Mg show a strong preference for incorporation of Mg^{2+} into the copiapite (Fig. 3*b*). These copiapite samples contain almost no Al^{3+}. Similarly, the samples more abundant in Al crystallized copiapite which contains almost no Mg^{2+}.

TABLE 3. Lattice parameters of the Fe^{3+}-Al copiapite phases synthesized at 75°C. The values in the parentheses are the estimated standard deviations. Column *A* specifies the composition at the *A* site. The lattice parameters *a*, *b*, *c* are in Å; α, β, γ are in degrees.

Sample	*A*	Type	*a*	*b*	*c*	α	β	γ	*V*
FAC-1	$Al_{0.59}Fe_{0.08}$	AL	7.3821(5)	18.225(2)	7.3235(5)	93.894(5)	102.214(5)	99.203(5)	945.3(1)
FAC-2	$Al_{0.59}Fe_{0.08}$	AL	7.3819(9)	18.233(3)	7.3221(9)	93.896(9)	102.208(8)	99.188(9)	945.6(2)
FAC-3	$Al_{0.56}Fe_{0.11}$	AL	7.3843(5)	18.229(2)	7.3258(5)	93.900(5)	102.212(5)	99.195(5)	946.1(1)
FAC-4	$Al_{0.53}Fe_{0.14}$	AL	7.3847(7)	18.235(2)	7.3246(7)	93.892(7)	102.210(7)	99.188(7)	946.3(2)
FAC-5	$Al_{0.50}Fe_{0.16}$	AL	7.3847(8)	18.238(2)	7.3242(8)	93.895(8)	102.213(7)	99.178(7)	946.4(2)
FAC-6	$Al_{0.44}Fe_{0.22}$	AL	7.3837(6)	18.247(2)	7.3230(6)	93.905(6)	102.209(5)	99.159(6)	946.7(2)
FAC-7	$Al_{0.35}Fe_{0.31}$	AL	7.3857(7)	18.264(2)	7.3250(7)	93.910(7)	102.214(6)	99.133(7)	948.2(2)
FAC-8	$Al_{0.27}Fe_{0.39}$	AL	7.3846(6)	18.273(2)	7.3238(6)	93.933(6)	102.201(6)	99.094(6)	948.5(2)
FAC-9	$Al_{0.14}Fe_{0.52}$	AL	7.3868(6)	18.313(2)	7.3264(6)	93.948(6)	102.211(5)	99.011(5)	951.4(1)
FAC-10	$Fe_{0.66}$	AL	7.3873(2)	18.356(1)	7.3280(2)	93.963(2)	102.202(2)	98.939(2)	954.1(1)

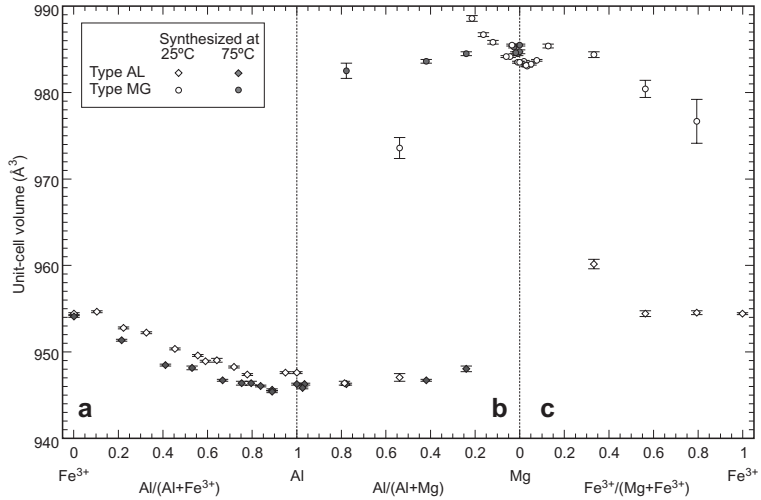

FIG. 3. Variation of unit-cell volume in the copiapite with the cations Fe^{3+}, Mg and Al in the *A* site.

Optical microscope observations do not show whether the varying compositions represent early and late phases. This evidence, as well as the strong enrichment of the single-phase samples in either Mg or Al, suggests that the system contains an immiscibility gap.

The samples synthesized at $T = 25$ºC also show a very strong tendency for incorporation of Mg^{2+} into copiapite. This tendency can easily be seen in Fig. 3*b*, where most points for the Mg-Al series cluster near the magnesiocopiapite end-member. The initial solutions, as mentioned above, were prepared at regularly incremented (0.1) Mg/(Mg+Al) intervals between the end-members. All the Mg-rich copiapite samples in this series belong to the structural type MG. The inclusion of a relatively small amount of Al^{3+} in the Mg-rich copiapite results in a rapid increase in the unit-cell volume. This increase continues to the sample with Mg/(Mg+Al) ≈ 0.8. The next sample shows significant anisotropic broadening of the diffraction peaks (Fig. 4*b*). The strongest broadening by far is observed for the 020 peaks, indicating disorder in the direction of the *b* axis. Disorder in this direction may be caused by re-arrangement of the infinite chains and the isolated

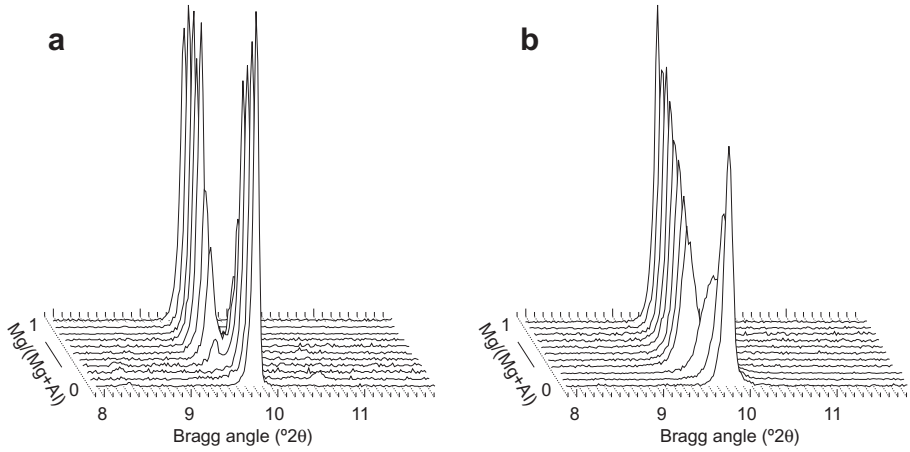

FIG. 4. The 002 peaks in the Mg-Al copiapite series prepared at (*a*) $T = 75$ºC or (*b*) $T = 25$ºC. The variable plotted on the vertical axis is intensity. All patterns were normalized to equal integral intensity.

TABLE 4. Lattice parameters of the Mg-Al copiapite phases synthesized at 75ºC. The values in the parentheses are the estimated standard deviations. Column *A* specifies the composition at the *A* site, the column Frac' gives the fraction of the phase in % in the two-phase samples. The lattice parameters *a*, *b*, *c* are in Å; α, β, γ are in degrees. Note that the samples do not strictly belong to a binary system magnesiocopiapite–aluminocopiapite because some of them contain a small amount of Fe^{3+} in the *A* site.

Sample	*A*	Type	Frac'	*a*	*b*	*c*	α	β	γ	*V*
MAC-1	$Al_{0.67}$	AL	100	7.3842(4)	18.233(1)	7.3249(3)	93.888(4)	102.215(3)	99.197(4)	946.2(1)
MAC-2	$Mg_{0.02}Al_{0.52}Fe_{0.14}$	AL	100	7.3830(4)	18.232(1)	7.3226(4)	93.895(4)	102.205(4)	99.189(4)	945.8(1)
MAC-3	$Mg_{0.02}Al_{0.50}Fe_{0.15}$	AL	100	7.3846(4)	18.236(1)	7.3242(4)	93.895(4)	102.210(4)	99.189(4)	946.3(1)
MAC-4	$Mg_{0.13}Al_{0.45}Fe_{0.13}$	AL	92	7.3833(4)	18.237(1)	7.3244(4)	93.895(4)	102.208(4)	99.174(4)	946.3(1)
		MG	8	7.340(4)	18.772(6)	7.392(4)	91.41(5)	102.10(4)	98.77(4)	982.5(8)
MAC-5	$Mg_{0.41}Al_{0.29}Fe_{0.10}$	AL	57	7.3817(7)	18.242(2)	7.3281(7)	93.900(8)	102.226(7)	99.190(7)	946.7(2)
		MG	43	7.3446(10)	18.793(2)	7.3891(10)	91.360(12)	102.13(1)	98.833(10)	983.7(2)
MAC-6	$Mg_{0.60}Al_{0.19}Fe_{0.07}$	MG	66	7.3450(7)	18.805(2)	7.3906(7)	91.378(9)	102.155(7)	98.816(7)	984.5(2)
		AL	34	7.3839(12)	18.248(3)	7.3334(11)	93.925(13)	102.23(1)	99.175(12)	948.0(3)
MAC-7	$Mg_{0.97}Al_{0.02}$	MG	100	7.3469(4)	18.806(1)	7.3904(4)	91.364(5)	102.166(4)	98.809(4)	984.7(1)
MAC-8	$Mg_{0.97}Al_{0.02}$	MG	100	7.3492(5)	18.806(1)	7.3918(5)	91.357(5)	102.164(4)	98.817(5)	985.2(1)
MAC-9	$Mg_{1.01}Al_{0.01}$	MG	100	7.3481(7)	18.797(2)	7.3917(7)	91.368(8)	102.172(7)	98.825(7)	984.5(2)
MAC-10	$Mg_{1.03}$	MG	100	7.3473(7)	18.799(2)	7.3928(7)	91.373(8)	102.173(7)	98.816(7)	984.7(2)
MAC-11	$Mg_{1.06}$	MG	100	7.3495(6)	18.807(2)	7.3933(6)	91.373(7)	102.169(6)	98.810(6)	985.5(2)

octahedra, reflecting the conflicting tendencies to build one or the other structural type of copiapite. It is difficult to determine with certainty from our XRD data whether the sample contains one, two or a series of disordered copiapite phases. In analogy with the samples prepared at 75ºC, we refer to the region where this disorder exists as the two-phase region. This term will be applied also to other copiapite systems showing similar behaviour, noting again that the precise number of phases cannot be determined reliably.

The Mg–Fe^{3+} join at 25°C

The two end-members in this series belong to two different structural types (AL and MG) and therefore immiscibility may be expected. The compositions more abundant in Mg belong to the structural type MG and show strong preference for the incorporation of Mg^{2+} over Fe^{3+} (Fig. 3*c*). Inclusion of Fe^{3+} into these phases leads to a sharp increase in the unit-cell volume, similar to the Mg-Al series. The samples with lower Mg/(Mg+Fe^{3+}) ratios at the *A* site belong to the two-phase field. The two-phase field covers most of the compositional space in this system (Fig. 3*c*), indicating that the mixing of Mg^{2+} and Fe^{3+} at the *A* site in copiapite is unfavourable to a large extent.

We have also attempted to synthesize this series at T = 75ºC. Although all solutions yielded copiapite, most of them were contaminated by a substantial amount of kornelite ($Fe_2(SO_4)_3(H_2O)_{\sim 7}$). The crystallization of kornelite depletes the system in Fe^{3+}. Hence, all copiapite crystals are shifted strongly towards more Mg-rich compositions and little can be learned about the Mg-Fe^{3+} solid solution or immiscibility among the copiapite phases. For this reason, the results from the series prepared at T = 75ºC are not reported here.

The Al–Fe^{2+} join at 25°C

Both end-members in this series belong to the structural type AL. However, the large difference in the ionic radii of Al^{3+} and Fe^{2+}, their different charge and the need to introduce vacancies along with Al^{3+} are the most likely causes for the existence of considerable disorder in several intermediate members. The compositions with Al/(Al+Fe^{2+}) between 1.0 and ~0.4 have unit-cell volumes slightly smaller than that of the Al-copiapite (Fig. 5*a*). These samples displayed a slight preference for Al^{3+} over Fe^{2+}. Significant broadening of the 020 peaks in the samples with Al/(Al+Fe^{2+}) between 0.4 and 0.1 indicates that multiple phases may be present. Nevertheless,

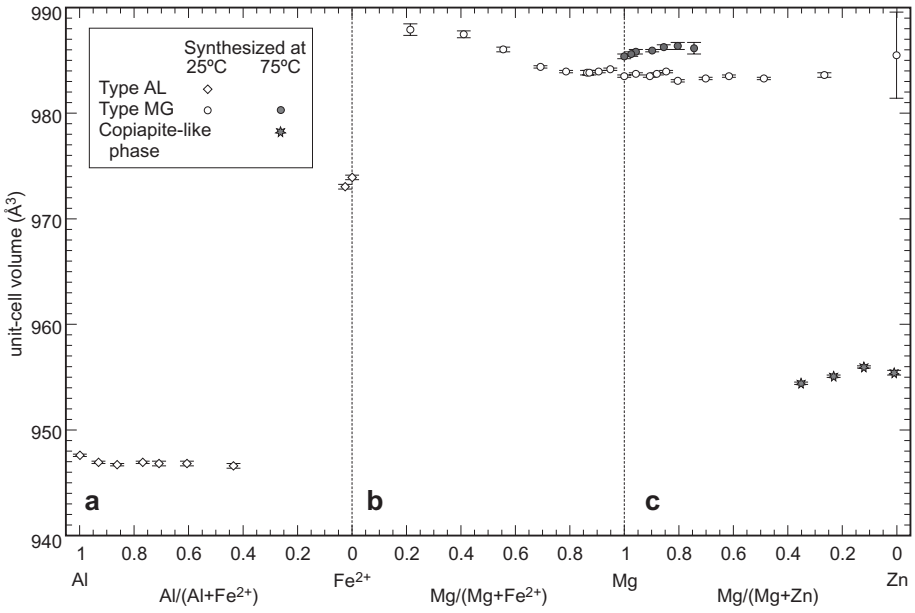

FIG. 5. Variation of the unit-cell volume (V) in the copiapite with the cations Al, Fe^{2+}, Mg and Zn in the *A* site. For the copiapite-like phase, V/2 is plotted.

attempts to refine the patterns with two copiapite phases always failed. The refinement accepted the two phases but diverged immediately if the peaks were allowed to broaden. Therefore, the precise nature of disorder in these phases or the number of phases in these samples remains unknown.

The Mg–Fe^{2+} join at 25°C

As the two end-members in this series belong to different structural types, the existence of a two-phase region is expected. However, none of the patterns along this join can be satisfactorily refined with two copiapite phases. The Mg-rich and intermediate compositions clearly belong to the type MG, with sharp peaks and unit-cell volumes (V) close to that of the end-member Mg-copiapite (Fig. 5*b*). As in other systems investigated here, the compositions more abundant in Mg display a pronounced preference for Mg^{2+} over the other cation present (Fe^{2+}). As the $Mg/(Mg+Fe^{2+})$ ratio decreases, V sharply increases. This increase is surprising since the two ions have the same charge and are similar in size. The rapid increase of V for Fe^{2+}-rich compositions and the simultaneous peak broadening in this series probably reflects the conflicting tendencies to accommodate both Mg^{2+} and Fe^{2+} in a single structural type of the copiapite structure. As stated above, the Fe^{2+}-copiapite belongs to the type AL and its V is markedly smaller than the V of any other member of this series (Fig. 5).

The Mg–Zn join at 25°C and 75°C

At T = 25ºC, the solid solution among the Mg and Zn end-members is continuous and belongs to the structural type MG. The copiapite phase shows strong preference for Mg over Zn during crystallization (Fig. 5*c*). As the concentration of Zn in copiapite increases, the crystallinity of the product decreases. This trend can be seen from the increasing errors on the results of the refinement towards the Zn-rich compositions (Fig. 5*c*).

At T = 75ºC, there is no continuous solid solution between the Mg and Zn end-members. The Mg-rich compositions precipitate a copiapite phase of the structural type MG. These phases also strongly prefer Mg over Zn and their unit-cell volume increases almost systematically up to Mg/(Mg+Zn) = 0.75. The compositions rich in Zn, however, crystallize a copiapite-like phase (Table 2). This phase is able to incorporate significantly more Zn than copiapite although it also shows a slight preference for Mg^{2+} over Zn^{2+}.

The ternary system Mg-Al-Fe^{3+} at 25°C

The co-existence of two copiapite phases along the Mg-Fe^{3+} and Mg-Al joins prompted us to explore the ternary system Mg-Al-Fe^{3+} copiapite in detail, with emphasis on mapping out the two-phase field. At 25ºC, the two-phase region covers most of the ternary system (Fig. 6). As in the binary systems, the copiapite phases show strong preference for Mg^{2+} and a slight one for Al^{3+}. The V of the copiapite phases is greatest for the phases most abundant in Mg^{2+} and smallest for the Al^{3+}-rich phases (see the supplementary Table S1, which can be found at http://www.minersoc.org/pages/ e_journals/dep_mat.html).

Natural samples

A small collection of natural samples which was amassed for this work served to test whether the two structural types determined in this study also

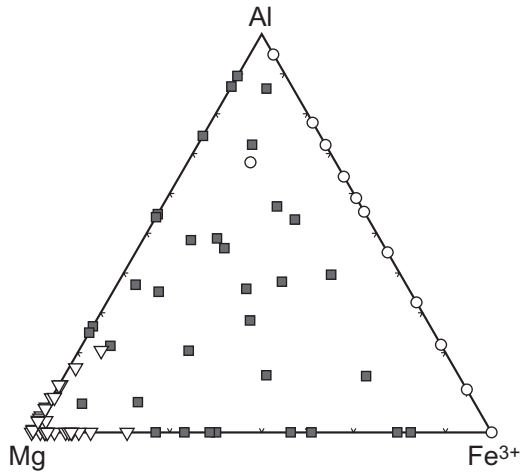

FIG. 6. A ternary plot showing the copiapite samples with a single phase of the type AL (open circles), single phase of the type MG (open inverted triangles) and samples with multiple copiapite phases (black squares). The plot shows the molar proportions of Mg, Al and Fe^{3+} at the A site in the copiapite structure. Note that for the samples with multiple copiapite phases, only the total chemical composition could be plotted. Because of their fine-grained nature, we were not able to determine the composition of the co-existing phases.

occur in nature. These natural samples were intended to cover a wide range of compositions. As with the synthetic samples, each of the natural samples can be assigned to the type MG or AL (Table 5). All XRD patterns of the natural samples had sharp, well defined peaks. No broadening similar to that found in the two-phase fields in our synthetic systems was detected. The small amount of material available and the presence of impurities (Table 5) precluded a precise determination of the chemical composition of the natural copiapite samples. For this reason, we abandoned the original idea to collect more natural copiapite specimens and turned most of our attention to the synthetic samples. It should also be noted that the sample 'Al-Mg copiapite' (see Table 5) does not represent an intermediate between the synthetic Al and Mg end-members. This sample was contaminated by pickeringite and was available in the least amounts. Whether the deviation from the Al-Mg binary system is caused by problems during the refinement owing to low intensities of the peaks or an additional chemical component in the copiapite crystals is unclear.

Infrared spectroscopy

The mid-IR spectra of all copiapite end-members synthesized in this study are very similar. They all display prominent stretching O–H vibrational (νOH) bands in the region of 3000–3600 cm^{-1}. These bands arise from the interaction of the IR radiation and the vibrational modes of water molecules (Ryskin, 1974). Because there are twenty water molecules in a unit cell of copiapite, there is a significant overlap and the νOH bands merge into a broad feature (Fig. 7). Some of these broad features include a relatively sharp peak at 3526 cm^{-1} that can be assigned to the single OH group in the structure. The bending H–O–H vibrations are manifested by a pronounced band at 1637 cm^{-1}.

The portion of the spectrum between 500–1200 cm^{-1} is dominated by sulphate vibrational bands. An undistorted SO_4 group with tetrahedral symmetry (point symmetry T_d) has four vibrational modes ν_1, ν_2, ν_3 and ν_4 with the corresponding irreducible representations of $A_1 + E + T_2 + T_2$. The symbols A, E and T represent singly, doubly and triply degenerate modes, respectively. The energy of these modes is: ν_1 983 cm^{-1}, ν_2 450 cm^{-1}, ν_3 1105 cm^{-1} and ν_4 611 cm^{-1}, respectively (Nakamoto, 1986).

TABLE 5. Lattice parameters (in Å and degrees), structural type and localities of the natural samples.

Sample locality Impurity (if present)	Type	*a*	*b*	*c*	α	β	γ	*V*
Zn-Mg copiapite Mazarron, Murcia (Spain)	MG	7.3417(8)	18.791(1)	7.3824(9)	91.416(11)	102.156(9)	98.871(9)	982.0(2)
Ferricopiapite Mina Sao Domingos, Mertola (Portugal)	AL	7.3951(2)	18.3435(4)	7.3352(2)	93.901(2)	102.200(2)	98.994(2)	955.3(1)
Paracoquimbite (*R*3̄)		10.9636(2)	10.9636(2)	51.484(1)	90	90	120	5359.2(2)
Al-Mg copiapite Valachov, Skřivaň (Czech Republic)	AL	7.329(7)	18.849(10)	7.343(6)	93.38(9)	102.43(9)	100.75(10)	968.0(14)
Pickeringite ($P2_1/c$)		6.1871(5)	24.272(2)	21.242(1)	90	100.339(6)	90	3138.3(4)
Mg-Al copiapite Denver mine, Santa Cruz Co, AZ (USA)	MG	7.3430(4)	18.7872(7)	7.3863(4)	91.361(5)	102.175(4)	98.828(4)	982.6(1)

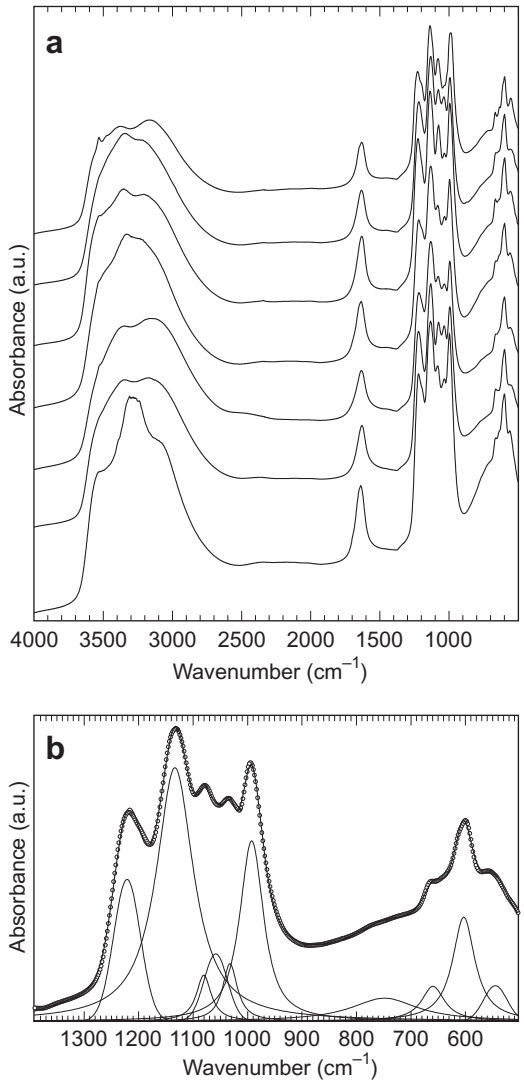

FIG. 7. (*a*) IR spectra of synthetic end-members; from bottom to top: HSC-1, HSC-11, HSC-21, HSC-106, HSC-116, HSC-128, HSC-79. (*b*) A portion of a spectrum of the sample HSC-21. The functions shown fit the measured spectrum and their positions are stated in the text. The linear background function used during fitting is not shown.

Distortion of the sulphate group to the point symmetry C_1 lifts the degeneracy and nine IR-active modes with the irreducible representations of A can be theoretically distinguished in a spectrum. Of these nine modes, seven fall in the spectral range of this study: three ν_3 modes, one ν_1 mode and three ν_4 modes. Therefore, three sulphate sites in the structure of copiapite, each with point symmetry C_1, should together produce 21 vibrational bands in the measured spectra. Because of the considerable overlap of these bands and an additional overlap with bending (δOH) O–H modes, not all these bands can be distinguished. In the region between 1400–900 cm^{-1}, twelve SO_4 and δOH bands are expected. A satisfactory fit of this region could be achieved with a set of six Gaussian functions centred at 992, 1035, 1061, 1081, 1135 and 1223 cm^{-1} (Fig. 7). In the region between 700–500 cm^{-1}, three SO_4 ν_4 triplets are expected. Three bands centred at 543, 603 and 659 cm^{-1} could be distinguished in this region by fitting (Fig. 7).

Discussion and conclusions

The two principal components of the copiapite structure, the infinite chains and the isolated *A* sites, are connected only by an intricate network of hydrogen bonds (Majzlan and Kiefer, 2006). The flexibility of this network and the consequent possibility of re-arranging these components is the reason the copiapite structure accepts a number of cations in the *A* site. The major differences between the structural type AL and MG are: (1) the size of the unit cell; (2) the orientation of the isolated octahedra $A(H_2O)_6$; and (3) the topology of the infinite chains (Fig. 1). The two smallest cations (Al^{3+}, ionic radius = 0.54 Å, Fe^{3+} 0.65 Å) form copiapite phases of the type AL with the smallest *V*. Surprisingly, the copiapite with the largest cation (Fe^{2+} 0.78 Å) belongs to the same structural type and its *V* is much smaller than that expected from a simple ionic-radius–*V* relationship. Copiapite with the other divalent cations (Mg^{2+} 0.72, Zn^{2+} 0.74, Ni^{2+} 0.69 Å) belongs to the structural type MG and the *V* is greater than that of the copiapite of the structural type AL. The unit-cell size is largely controlled by the value of the lattice parameter *b*. These cluster around values of 18.2–18.4 Å for the structural type AL and 18.7–18.85 Å for the structural type MG (Fig. 8). The outliers of these ranges are the samples in the two-phase fields where significant disorder exists. The lattice parameters *a*, *c*, α, β and γ vary within relatively narrow bounds and influence the *V* much less than *b* (Fig. 8).

The greatest changes occur in the *b* direction, meaning that the factor controlling the structural type and the unit-cell size is the orientation and size of the isolated octahedra $A(H_2O)_6$. Although the infinite chains also change their topology in

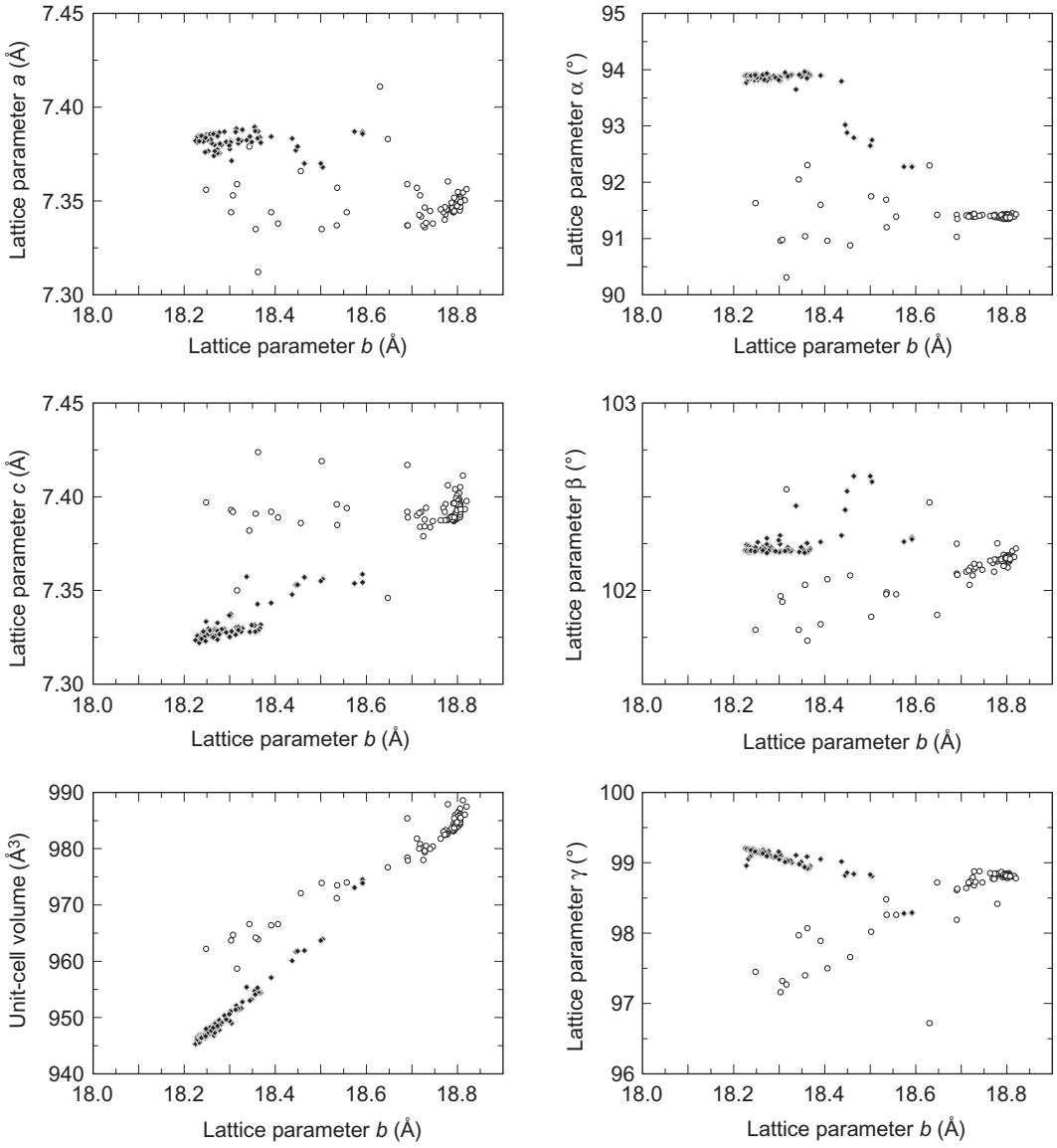

FIG. 8. Variation of the lattice parameters and the unit-cell volume in the synthesized copiapite samples. Grey diamonds – structural type MG, open circles – structural type AL.

response to the re-orientation of the isolated octahedra (Fig. 1), the repeat period of the chains varies no more than a few hundreths of an angström (9.25–9.27 Å).

When forced to form a solid solution, the copiapite phases respond in a variety of ways:

(1) Formation of a complete solid solution (Fe^{3+}–Al solution, 25ºC or 75ºC).

(2) Immiscibility (Mg–Al solution, 75ºC).

(3) Development of a field where one, two or multiple disordered phases may exist (e.g. Mg–Al, Mg–Fe^{3+}, Al–Fe^{2+} solutions, 25ºC).

(4) Abrupt change from copiapite to a copiapite-like phase (Mg–Zn, Mg–Ni solution, 75ºC).

(5) Abrupt change from one structural type to the other (Mg–Fe^{2+} solution, 25ºC).

The use of a full-profile Rietveld refinement proved to be crucial as only this method was able to address the fine structural differences described in this study, as well as providing reliable lattice parameters for the triclinic unit cell and correcting for small systematic errors (especially the horizontal displacement of the specimens). The discrepancies in the previous structural studies of the copiapite phases are, in our opinion, the consequence of not using a full-profile analysis of the powder XRD patterns.

The subtle structural differences between the structural types MG, AL and the copiapite-like phase (CL) cannot be distinguished in the IR spectra. This close similarity of the spectra suggests that the copiapite-like phase comprises the same structural segments (polyhedral chains, isolated sites, water molecules) as the structure of copiapite itself. In all cases, the number of bands is too large and the overlap too strong to assign the individual bands to the theoretically predicted vibrational modes.

Overall, the phases that belong to the copiapite group form an exceedingly complicated system. The understanding of this system may aid in the comprehension of acid mine-drainage pollution where copiapite commonly occurs. We plan to continue with thermochemical studies of this system in order to describe the thermodynamic properties of the individual end-members and the solid solutions.

Acknowledgements

This work was supported financially by Deutsche Forschungsgemeinschaft, grant no. MA3927/2-1. We are grateful to S. Hirth-Walther and R. Bolanz for their help with the wet chemical analyses of the copiapite samples. We thank P. Stephens (National Synchrotron Light Source, Brookhaven National Laboratory, NY, USA) for help with the XRD experiments at the X16 beamline at NSLS. Use of the NSLS was supported by the U.S. Department of Energy, Office of Science, Office of Basic Energy Sciences, under Contract No. DE-AC02-98CH10886. We acknowledge the ANKA Angstroemquelle Karlsruhe (Forschungszentrum Karlsruhe, Germany) for the provision of beam-time and we thank S. Doyle for assistance using beamline DIFF. We also thank B. Gasharova for access to the infrared spectrometer at ANKA. We are grateful to M. Wang at the Swiss Light Source (Paul Scherrer Institute, Villigen, Switzerland) for the opportunity to use the beamline X06SA.

References

Atencio, D., Carvalho, F.M.S. and Hypolito, R. (1996) Synthesis and X-ray powder diffraction data for Mg-, Al- and Ni- end-members of the copiapite group. *Anais da Associacao Brasileira de Quimica*, **45**, 66–72.

Bayliss, P. and Atencio, D. (1985) X-ray powder diffraction data and cell parameters for copiapite-group minerals. *The Canadian Mineralogist*, **23**, 53–56.

Broemme, B. and Poellmann, H. (2007) Synthesis, crystal structure and application of compounds with copiapite and voltaite structure. *Geochimica et Cosmochimica Acta*, **71**, Special Supplement 15S, A123.

Fanfani, L., Nunzi, A., Zanazzi, P.F. and Zanzari, A.R. (1973) The copiapite problem: the crystal structure of a ferrian copiapite. *American Mineralogist*, **58**, 314–322.

Friedlander, L.R., Tosca, N.J. and Arvidson, R.E. (2007) Preliminary experiments in the systematic investigations of the spectroscopic properties of synthetic copiapite group minerals. *Lunar and Planetary Science Conference*, **XXXVIII**, 2049.

Haidinger, W. (1845) *Handbuch der bestimmenden Mineralogie*. Braumüller & Seidel, Wien.

Jamieson, H.E., Robinson, C., Alpers, C.N., McCleskey, R.B., Nordstrom, D.K. and Peterson, R.C. (2005) Major and trace element composition of copiapite-group minerals and coexisting water from the Richmond mine, Iron Mountain, California. *Chemical Geology*, **215**, 387–405.

Johansson, G. (1962) On the crystal structures of $FeOHSO_4$ and $InOHSO_4$. *Acta Chemica Scandinavica*, **16**, 1234–1244.

Larson, A.C. and von Dreele, R.B. (1994) *GSAS. General Structure Analysis System*. LANSCE, MS-H805, Los Alamos, New Mexico.

Majzlan, J. and Kiefer, B. (2006) An X-ray- and neutron-diffraction study of synthetic ferricopiapite, $Fe_{14/3}(SO_4)_6(OD,OH)_2(D_2O,H_2O)_{20}$, and *ab initio* calculations on the structure of magnesiocopiapite, $MgFe_4(SO_4)_6(OH)_2(H_2O)_{20}$. *The Canadian Mineralogist*, **44**, 1227–1237.

Nakamoto, K. (1986) *Infrared and Raman spectra of inorganic and coordination compounds*. John Wiley, New York.

Posnjak, E. and Merwin, H.E. (1922) The system, Fe_2O_3-SO_3-H_2O. *Journal of the American Chemical Society*, **44**, 1965–1994.

Quartieri, S., Triscari, M. and Viani, A. (2000) Crystal structure of the hydrated sulphate pickeringite ($MgAl_2(SO_4)_4{\cdot}22H_2O$): X-ray powder diffraction study. *European Journal of Mineralogy*, **12**, 1131–1138.

Rammelsberg, C.F. (1860) *Handbuch der*

Mineralchemie. Verlag von Wilhelm Engelman, Leipzig.

Robinson, P.D. and Fang, J.H. (1971) Crystal structures and mineral chemistry of hydrated ferric sulphates: II. The crystal structure of paracoquimbite. *American Mineralogist*, **56**, 1567–1571.

Rose, H. (1833) Ueber einige in Südamerika vorkommende Eisenoxydsalze. *Annalen der Physik*, **27**, 309–319.

Ryskin, Ya.I. (1974) The vibrations of protons in minerals: hydroxyl, water and ammonium. Pp. 137–181 in: *The Infrared Spectra of Minerals* (V.C. Farmer, editor). Monograph **4**. Mineralogical Society, London.

Scharizer, R. (1913) Beiträge zur Kenntnis der chemischen Constitution und der Genese der natürlichen Ferrisulphate VIII. *Zeitschrift für Kristallographie, Kristallgeometrie, Kristallphysik, Kristallchemie*, **52**, 372–398.

Süsse, P. (1972) Crystal structure and hydrogen bonding of copiapite. *Zeitschrift für Kristallographie*, **135**, 34–55.

Visser, J.W. (1969) A fully automatic program for finding the unit cell from powder data. *Journal of Applied Crystallography*, **2**, 89–95.

Walter-Levy, L. and Quemeneur, E. (1963) Sur la thermolyse du sulphate ferrique basique $6Fe_2(SO_4)_3,Fe_2O_3.nH_2O$. *Comptes Rendus Academy of Science Paris*, **257**, 3410–3413.

Table S1. Supplementary information to the manuscript by Majzlan and Michallik (*Mineralogical Magazine*). Listed in the sample ID, the amount of chemicals (deionized water and sulfates of Mg, Fe^{3+}, Al, Ni, Zn, and Fe^{2+}) used to produce the sample; the temperature of synthesis in ºC; the expected and measured stoichiometry at the *A* site in copiapite according to the general formula $AFe_4(SO_4)_6(OH)_2(H_2O)_{20}$; the structural type of the phase synthesized: **MG** = structural type **MG**, **AL** = structural type **AL**; **CL** = copiapite-like phase; and the lattice parameters of all phases identified in the samples. The values χ^2 and wR_p describe the goodness of the fit and are defined in the technical manual for GSAS (see Larson and von Dreele 1994). For the samples of the type **MG** and **AL**, these values refer to the results of the Rietveld refinement. For samples of the type **CL**, these values refer to the results of the LeBail refinement.

	amount of sulfates weighed out (g)				expected stoichiometry at the *A* site				measured stoichiometry at the A site				lattice parameters (Å, º) and unit cell volume (Å^3) for one or two phases in the sample, as applicable							
sample	water (mL) T (ºC)	Mg Ni	Fe^{3+} Zn	Al Fe^{2+}	Mg Ni	Fe^{3+} Zn	Al Fe^{2+}		Mg Ni	Fe^{3+} Zn	Al Fe^{2+}		type	*a*	*b*	*c*	α	β	γ	*V*	χ^2 wRp
HSC-1	1.20 25	0.4779 0	2.0221 0	0 0	1.000 0	0 0	0 0		1.017 0	0 0	0 0		**MG**	7.3451(4)	18.7936(11)	7.3891(4)	91.369(5)	102.169(4)	98.831(4)	983.58(10)	3.81 0.2826
HSC-2	1.20 25	0.4325 0	2.0675 0	0 0	0.900 0	0.067 0	0 0		0.972 0	0.019 0	0 0		**MG**	7.3451(4)	18.7940(10)	7.3886(4)	91.373(5)	102.163(4)	98.822(4)	983.60(9)	2.74 0.2486
HSC-3	1.20 25	0.3867 0	2.1133 0	0 0	0.800 0	0.133 0	0 0		0.958 0	0.028 0	0 0		**MG**	7.3444(4)	18.7921(10)	7.3870(4)	91.364(4)	102.163(4)	98.829(4)	983.16(9)	3.07 0.2581
HSC-4	1.20 25	0.3403 0	2.1597 0	0 0	0.700 0	0.200 0	0 0		0.951 0	0.033 0	0 0		**MG**	7.3440(5)	18.7912(13)	7.3879(5)	91.370(5)	102.168(4)	98.824(5)	983.17(11)	4.44 0.3037
HSC-5	1.20 25	0.2933 0	2.2067 0	0 0	0.600 0	0.267 0	0 0		0.927 0	0.048 0	0 0		**MG**	7.3446(4)	18.7911(11)	7.3886(4)	91.375(5)	102.165(4)	98.828(4)	983.34(10)	2.50 0.2350
HSC-6	1.20 25	0.2459 0	2.2541 0	0 0	0.500 0	0.333 0	0 0		0.893 0	0.071 0	0 0		**MG**	7.3457(5)	18.7943(12)	7.3893(5)	91.371(5)	102.174(4)	98.817(4)	983.75(11)	2.78 0.2494
HSC-7	1.20 25	0.1978 0	2.3022 0	0 0	0.400 0	0.400 0	0 0		0.819 0	0.120 0	0 0		**MG**	7.3493(9)	18.7995(22)	7.3957(9)	91.406(9)	102.176(8)	98.789(8)	985.38(20)	3.69 0.2865
HSC-8	1.20 25	0.1492 0	2.3508 0	0 0	0.300 0	0.467 0	0 0		0.573 0	0.285 0	0 0		**MG** **AL**	7.3440(16) 7.3833(26)	18.791(4) 18.437(6)	7.3965(17) 7.3478(24)	91.433(18) 93.795(29)	102.160(15) 102.294(27)	98.795(15) 99.016(28)	984.4(4) 960.1(6)	3.60 0.2844
HSC-9	1.20 25	0.1001 0	2.3999 0	0 0	0.200 0	0.533 0	0 0		0.341 0	0.440 0	0 0		**MG** **AL**	7.338(4) 7.3811(16)	18.746(8) 18.368(5)	7.387(4) 7.3317(16)	91.42(5) 93.901(17)	102.11(4) 102.224(16)	98.72(4) 98.953(17)	980.4(9) 954.4(4)	5.16 0.3358
HSC-10	1.20 25	0.0503 0	2.4497 0	0 0	0.100 0	0.600 0	0 0		0.147 0	0.569 0	0 0		**MG** **AL**	7.383(11) 7.3839(10)	18.647(22) 18.3662(28)	7.346(11) 7.3298(10)	91.42(15) 93.922(10)	101.87(12) 102.215(9)	98.72(13) 98.926(10)	976.7(25) 954.47(24)	3.87 0.2996
HSC-11	1.20 25	0 0	2.5000 0	0 0	0 0	0.667 0	0 0		0 0	0.667 0	0 0		**AL**	7.3871(5)	18.3622(13)	7.3286(4)	93.938(5)	102.208(4)	98.920(4)	954.53(11)	2.86 0.2576
HSC-12	1.20 25	0.4311 0	2.0269 0	0.0420 0	0.900 0	0 0	0.067 0		1.008 0	0 0	0.007 0		**MG**	7.3450(5)	18.7926(12)	7.3882(5)	91.369(5)	102.164(4)	98.825(5)	983.44(11)	3.18 0.2600
HSC-13	1.20 25	0.3841 0	2.0317 0	0.0842 0	0.800 0	0 0	0.133 0		0.966 0	0 0	0.041 0		**MG**	7.3466(5)	18.7980(12)	7.3908(5)	91.377(5)	102.166(5)	98.828(5)	984.26(11)	2.39 0.2339
HSC-14	1.20 25	0.3369 0	2.0365 0	0.1266 0	0.700 0	0 0	0.200 0		0.908 0	0 0	0.061 0		**MG**	7.3467(5)	18.7951(13)	7.3906(5)	91.371(6)	102.177(5)	98.820(5)	984.08(12)	2.64 0.2438
HSC-15	1.20 25	0.2894 0	2.0413 0	0.1692 0	0.600 0	0 0	0.267 0		0.964 0	0 0	0.036 0		**MG**	7.3509(6)	18.8015(15)	7.3943(6)	91.369(6)	102.184(5)	98.809(6)	985.47(14)	2.91 0.2058
HSC-16	1.20 25	0.2418 0	2.0462 0	0.2120 0	0.500 0	0 0	0.333 0		0.826 0	0.004 0	0.112 0		**MG**	7.3505(8)	18.8031(19)	7.3970(8)	91.373(8)	102.186(7)	98.815(7)	985.84(18)	3.90 0.2367
HSC-17	1.20 25	0.1939 0	2.0511 0	0.2550 0	0.400 0	0 0	0.400 0		0.756 0	0.013 0	0.149 0		**MG**	7.3520(11)	18.8040(27)	7.4019(11)	91.397(11)	102.187(10)	98.801(10)	986.75(25)	4.54 0.2535

sample	water (mL) T (ºC)	amount of sulfates weighed out (g) Mg Ni	Fe^{3+} Zn	Al Fe^{2+}	expected stoichiometry at the *A* site Mg Ni	Fe^{3+} Zn	Al Fe^{2+}	measured stoichiometry at the A site Mg Ni	Fe^{3+} Zn	Al Fe^{2+}	type	lattice parameters (Å, º) and unit cell volume (Å^3) for one or two phases in the sample, as applicable *a*	*b*	*c*	α	β	γ	*V*	χ^2 wRp
HSC-18	1.20	0.1458	2.0560	0.2982	0.300	0	0.467	0.662	0.043	0.182	**MG**	7.3545(18)	18.812(4)	7.4113(18)	91.453(18)	102.211(16)	98.805(16)	988.6(4)	6.52
	25	0	0	0	0	0	0	0	0	0									0.3026
HSC-19	1.20	0.0974	2.0609	0.3417	0.200	0	0.533	0.319	0.081	0.373	**AL**	7.3766(20)	18.253(6)	7.3296(20)	93.819(22)	102.258(19)	99.144(19)	947.0(5)	7.08
	25	0	0	0	0	0	0	0	0	0	**MG**	7.357(5)	18.536(11)	7.385(6)	91.20(6)	101.99(6)	98.26(6)	973.5(12)	0.3155
HSC-20	1.20	0.0488	2.0659	0.3853	0.100	0	0.600	0.132	0.097	0.482	**AL**	7.3760(12)	18.246(3)	7.3279(11)	93.816(12)	102.231(11)	99.153(11)	946.41(27)	5.61
	25	0	0	0	0	0	0	0	0	0									0.2800
HSC-21	1.20	0	2.0709	0.4291	0	0	0.667	0	0.034	0.632	**AL**	7.3853(7)	18.2486(18)	7.3280(6)	93.873(7)	102.221(6)	99.163(6)	947.65(16)	3.99
	25	0	0	0	0	0	0	0	0	0									0.2544
HSC-22	1.20	0	2.1125	0.3875	0	0.067	0.600	0	0.148	0.518	**AL**	7.3835(7)	18.2502(20)	7.3270(7)	93.866(8)	102.221(7)	99.154(7)	947.42(17)	6.41
	25	0	0	0	0	0	0	0	0	0									0.3080
HSC-23	1.20	0	2.1544	0.3456	0	0.133	0.533	0	0.186	0.481	**AL**	7.3856(8)	18.2569(21)	7.3287(8)	93.864(8)	102.216(7)	99.160(7)	948.25(18)	4.47
	25	0	0	0	0	0	0	0	0	0									0.2607
HSC-24	1.20	0	2.1965	0.3035	0	0.200	0.467	0	0.239	0.428	**AL**	7.3860(8)	18.2670(22)	7.3293(8)	93.882(8)	102.214(7)	99.129(8)	948.98(19)	3.72
	25	0	0	0	0	0	0	0	0	0									0.2454
HSC-25	1.20	0	2.2390	0.2610	0	0.267	0.400	0	0.274	0.392	**AL**	7.3857(6)	18.2680(16)	7.3284(6)	93.889(6)	102.214(5)	99.122(5)	948.87(13)	3.21
	25	0	0	0	0	0	0	0	0	0									0.2286
HSC-26	1.20	0	2.2818	0.2182	0	0.333	0.333	0	0.297	0.369	**AL**	7.3865(4)	18.2770(11)	7.3283(4)	93.887(4)	102.209(4)	99.101(4)	949.53(10)	2.57
	25	0	0	0	0	0	0	0	0	0									0.1969
HSC-27	1.20	0	2.3248	0.1752	0	0.400	0.267	0	0.366	0.301	**AL**	7.3869(4)	18.2883(12)	7.3293(4)	93.888(4)	102.212(4)	99.079(4)	950.35(10)	2.39
	25	0	0	0	0	0	0	0	0	0									0.1916
HSC-28	1.20	0	2.3682	0.1318	0	0.467	0.200	0	0.449	0.218	**AL**	7.3885(5)	18.3142(13)	7.3304(4)	93.900(5)	102.217(5)	99.038(5)	952.13(11)	2.62
	25	0	0	0	0	0	0	0	0	0									0.2066
HSC-29	1.20	0	2.4118	0.0882	0	0.533	0.133	0	0.520	0.147	**AL**	7.3880(4)	18.3277(12)	7.3298(4)	93.912(5)	102.213(4)	99.002(4)	952.78(10)	2.71
	25	0	0	0	0	0	0	0	0	0									0.2070
HSC-30A	1.20	0	2.4557	0.0443	0	0.600	0.067	0	0.595	0.072	**AL**	7.3894(5)	18.3546(14)	7.3314(5)	93.919(5)	102.215(5)	98.943(5)	954.73(11)	3.18
	25	0	0	0	0	0	0	0	0	0									0.2238
HSC-30B	1.20	0.3900	2.0678	0.0422	0.810	0.060	0.067	1.002	0	0.005	**MG**	7.3463(4)	18.7948(11)	7.3894(4)	91.365(5)	102.170(4)	98.826(4)	983.87(10)	3.68
	25	0	0	0	0	0	0	0	0	0									0.2269
HSC-31	1.20	0.3484	2.1091	0.0424	0.720	0.120	0.067	0.955	0	0.030	**MG**	7.3467(4)	18.7979(11)	7.3906(4)	91.364(5)	102.169(4)	98.819(4)	984.26(10)	3.29
	25	0	0	0	0	0	0	0	0	0									0.2173
HSC-32	1.20	0.3064	2.1509	0.0427	0.630	0.180	0.067	0.914	0	0.057	**MG**	7.3475(4)	18.7972(11)	7.3911(4)	91.368(5)	102.178(4)	98.819(4)	984.36(10)	3.32
	25	0	0	0	0	0	0	0	0	0									0.2187
HSC-33	1.20	0.2640	2.1931	0.0429	0.540	0.240	0.067	0.957	0.029	0	**MG**	7.3468(4)	18.7958(11)	7.3909(4)	91.371(5)	102.172(4)	98.820(4)	984.18(10)	3.53
	25	0	0	0	0	0	0	0	0	0									0.2228
HSC-34	1.20	0.2212	2.2357	0.0431	0.450	0.300	0.067	0.933	0.016	0.029	**MG**	7.3494(5)	18.8015(13)	7.3928(5)	91.373(5)	102.178(5)	98.815(5)	985.09(12)	3.26
	25	0	0	0	0	0	0	0	0	0									0.2151
HSC-35	1.20	0.1779	2.2788	0.0433	0.360	0.360	0.067	0.797	0.068	0.067	**AL**	7.368(6)	18.504(12)	7.356(5)	92.75(6)	102.58(7)	98.81(6)	963.9(12)	3.72
	25	0	0	0	0	0	0	0	0	0	**MG**	7.3495(9)	18.8005(22)	7.3981(9)	91.414(10)	102.167(9)	98.813(8)	985.75(21)	0.2352
HSC-36	1.20	0.1341	2.3223	0.0436	0.270	0.420	0.067	0.499	0.334	0	**AL**	7.3843(19)	18.391(5)	7.3433(18)	93.896(20)	102.260(19)	99.051(20)	957.1(4)	4.22
	25	0	0	0	0	0	0	0	0	0	**MG**	7.3429(16)	18.774(4)	7.3961(17)	91.426(19)	102.158(16)	98.786(16)	983.3(4)	0.2512
HSC-37	1.20	0.0899	2.3663	0.0438	0.180	0.480	0.067	0.300	0.467	0	**AL**	7.3814(10)	18.3483(27)	7.3315(10)	93.879(10)	102.232(9)	99.011(10)	953.19(23)	3.50
	25	0	0	0	0	0	0	0	0	0	**MG**	7.336(3)	18.728(5)	7.3879(29)	91.44(4)	102.113(28)	98.68(3)	979.4(6)	0.2283

		amount of sulfates weighed out (g)			expected stoichiometry at the *A* site			measured stoichiometry at the A site				lattice parameters (Å, º) and unit cell volume (Å^3) for one or two phases in the sample, as applicable							
sample	water (mL) T (ºC)	Mg Ni	Fe^{3+} Zn	Al Fe^{2+}	Mg Ni	Fe^{3+} Zn	Al Fe^{2+}	Mg Ni	Fe^{3+} Zn	Al Fe^{2+}	type	*a*	*b*	*c*	α	β	γ	*V*	χ^2 wRp
HSC-38	1.20	0.0452	2.4108	0.0440	0.090	0.540	0.067	0.124	0.584	0	**AL**	7.3844(6)	18.3442(17)	7.3279(6)	93.910(7)	102.206(6)	98.980(6)	953.03(14)	2.55
	25	0	0	0	0	0	0	0	0	0	**MG**	7.335(5)	18.502(9)	7.419(5)	91.75(6)	101.86(6)	98.02(5)	973.9(11)	0.1991
HSC-39	1.20	0.3432	2.0722	0.0846	0.711	0.059	0.133	0.874	0.084	0	**MG**	7.3469(4)	18.7969(10)	7.3902(4)	91.366(4)	102.170(4)	98.822(4)	984.18(9)	3.09
	25	0	0	0	0	0	0	0	0	0									0.2113
HSC-40	1.20	0.3018	2.1132	0.0851	0.622	0.119	0.133	0.884	0.078	0	**MG**	7.3479(4)	18.7974(10)	7.3917(4)	91.370(5)	102.172(4)	98.825(4)	984.52(10)	2.88
	25	0	0	0	0	0	0	0	0	0									0.2054
HSC-41	1.20	0.2600	2.1545	0.0855	0.533	0.178	0.133	0.854	0.098	0	**MG**	7.3467(4)	18.7977(11)	7.3908(4)	91.364(5)	102.171(4)	98.821(4)	984.27(10)	3.21
	25	0	0	0	0	0	0	0	0	0									0.2171
HSC-42	1.20	0.2178	2.1963	0.0859	0.444	0.237	0.133	0.718	0.188	0	**MG**	7.3492(6)	18.8024(15)	7.3956(6)	91.388(7)	102.176(6)	98.816(6)	985.46(14)	3.72
	25	0	0	0	0	0	0	0	0	0									0.2320
HSC-43	1.20	0.1751	2.2385	0.0864	0.356	0.296	0.133	0.644	0.237	0	**AL**	7.370(4)	18.464(10)	7.357(4)	92.79(5)	102.61(5)	98.84(5)	961.9(9)	5.22
	25	0	0	0	0	0	0	0	0	0	**MG**	7.3474(13)	18.799(3)	7.4006(13)	91.436(13)	102.155(12)	98.839(12)	985.68(29)	0.2707
HSC-44	1.20	0.1320	2.2812	0.0868	0.267	0.356	0.133	0.514	0.324	0	**AL**	7.3834(19)	18.361(5)	7.3427(18)	93.848(21)	102.253(19)	99.087(20)	955.3(4)	4.60
	25	0	0	0	0	0	0	0	0	0	**MG**	7.3440(19)	18.769(4)	7.3940(20)	91.408(22)	102.147(18)	98.775(19)	983.0(4)	0.2614
HSC-45	1.20	0.0885	2.3242	0.0873	0.178	0.415	0.133	0.324	0.340	0.111	**AL**	7.3808(10)	18.3189(29)	7.3304(10)	93.859(11)	102.231(10)	99.043(10)	951.38(24)	3.62
	25	0	0	0	0	0	0	0	0	0	**MG**	7.337(3)	18.690(6)	7.392(3)	91.42(4)	102.09(3)	98.61(3)	978.4(7)	0.2340
HSC-46	1.20	0.0445	2.3678	0.0877	0.089	0.474	0.133	0.144	0.469	0.101	**AL**	7.3822(7)	18.3251(19)	7.3280(6)	93.898(7)	102.210(6)	99.030(6)	951.62(16)	2.87
	25	0	0	0	0	0	0	0	0	0	**MG**	7.366(4)	18.456(8)	7.386(4)	90.88(6)	102.08(5)	97.66(5)	972.1(9)	0.2123
HSC-47	1.20	0.2962	2.0765	0.1272	0.613	0.058	0.200	0.971	0	0.028	**MG**	7.3471(4)	18.7959(10)	7.3907(4)	91.366(4)	102.172(4)	98.824(4)	984.20(9)	3.13
	25	0	0	0	0	0	0	0	0	0									0.2108
HSC-48	1.20	0.2552	2.1169	0.1279	0.525	0.117	0.200	0.973	0.035	0	**MG**	7.3459(4)	18.7948(11)	7.3901(4)	91.370(5)	102.172(4)	98.827(4)	983.90(10)	3.59
	25	0	0	0	0	0	0	0	0	0									0.2268
HSC-49	1.20	0.2137	2.1577	0.1285	0.438	0.175	0.200	0.877	0	0.083	**MG**	7.3484(7)	18.8001(18)	7.3929(7)	91.388(8)	102.179(6)	98.821(7)	984.85(16)	4.21
	25	0	0	0	0	0	0	0	0	0									0.2525
HSC-50	1.20	0.1719	2.1990	0.1292	0.350	0.233	0.200	0.647	0	0.235	**AL**	7.370(4)	18.500(9)	7.355(3)	92.65(4)	102.61(5)	98.83(4)	963.7(9)	4.73
	25	0	0	0	0	0	0	0	0	0	**MG**	7.3479(13)	18.804(3)	7.3989(13)	91.426(14)	102.156(13)	98.854(12)	985.7(3)	0.2645
HSC-51	1.20	0.1295	2.2406	0.1298	0.263	0.292	0.200	0.489	0.034	0.307	**AL**	7.3714(18)	18.304(5)	7.3282(17)	93.870(19)	102.208(18)	99.097(18)	949.0(4)	5.33
	25	0	0	0	0	0	0	0	0	0	**MG**	7.337(3)	18.725(7)	7.379(3)	91.39(4)	102.08(3)	98.79(3)	978.0(7)	0.2797
HSC-52	1.20	0.0868	2.2827	0.1305	0.175	0.350	0.200	0.195	0.260	0.277	**AL**	7.3828(7)	18.3189(20)	7.3289(7)	93.882(7)	102.215(7)	99.023(7)	951.52(17)	3.09
	25	0	0	0	0	0	0	0	0	0	**MG**	7.353(4)	18.718(7)	7.384(4)	91.42(5)	102.03(4)	98.71(4)	980.8(8)	0.2182
HSC-53	1.20	0.0436	2.3252	0.1312	0.088	0.408	0.200	0.130	0.177	0.403	**AL**	7.3777(7)	18.3000(21)	7.3252(7)	93.876(8)	102.206(7)	99.050(7)	949.38(17)	3.77
	25	0	0	0	0	0	0	0	0	0	**MG**	7.357(4)	18.711(7)	7.390(4)	91.41(5)	102.10(5)	98.64(5)	981.8(9)	0.2424
HSC-54	1.20	0.2493	2.0806	0.1700	0.514	0.057	0.267	0.832	0	0.112	**MG**	7.3475(5)	18.7981(12)	7.3920(5)	91.369(5)	102.174(4)	98.826(5)	984.52(11)	3.09
	25	0	0	0	0	0	0	0	0	0									0.2139
HSC-55	1.20	0.2088	2.1203	0.1709	0.429	0.114	0.267	0.866	0.005	0.084	**MG**	7.3494(8)	18.8005(19)	7.3958(8)	91.384(8)	102.184(7)	98.826(7)	985.34(18)	4.48
	25	0	0	0	0	0	0	0	0	0									0.2551
HSC-56	1.20	0.1679	2.1604	0.1717	0.343	0.171	0.267	0.666	0	0.222	**AL**	7.377(4)	18.445(9)	7.353(3)	93.02(4)	102.43(4)	98.82(4)	961.7(8)	5.13
	25	0	0	0	0	0	0	0	0	0	**MG**	7.3470(14)	18.797(3)	7.3992(15)	91.406(15)	102.188(13)	98.826(13)	985.3(3)	0.2727
HSC-57	1.20	0.1265	2.2009	0.1726	0.257	0.229	0.267	0.356	0	0.432	**AL**	7.3819(18)	18.302(5)	7.3364(18)	93.864(19)	102.248(18)	99.119(18)	951.1(4)	4.71
	25	0	0	0	0	0	0	0	0	0	**MG**	7.3383(29)	18.731(6)	7.3941(29)	91.39(3)	102.124(27)	98.728(28)	980.5(6)	0.2716
HSC-58	1.20	0.0848	2.2418	0.1734	0.171	0.286	0.267	0.267	0.216	0.272	**AL**	7.3799(10)	18.282(3)	7.3293(10)	93.841(11)	102.232(10)	99.101(10)	949.05(25)	4.15
	25	0	0	0	0	0	0	0	0	0	**MG**	7.344(4)	18.557(7)	7.394(4)	91.39(4)	101.98(4)	98.26(4)	974.0(8)	0.2489

sample	water (mL) T (ºC)	amount of sulfates weighed out (g) Mg Ni	Fe^{3+} Zn	Al Fe^{2+}	expected stoichiometry at the *A* site Mg Ni	Fe^{3+} Zn	Al Fe^{2+}	measured stoichiometry at the A site Mg Ni	Fe^{3+} Zn	Al Fe^{2+}	type	lattice parameters (Å, º) and unit cell volume (Å^3) for one or two phases in the sample, as applicable *a*	*b*	*c*	α	β	γ	*V*	χ^2 wRp
HSC-59	1.20	0.0426	2.2831	0.1743	0.086	0.343	0.267	0.106	0.318	0.278	**AL**	7.3815(8)	18.2921(22)	7.3276(8)	93.860(8)	102.210(8)	99.089(7)	949.66(18)	3.56
	25	0	0	0	0	0	0	0	0	0	**MG**	7.379(4)	18.343(8)	7.382(4)	92.05(5)	101.79(5)	97.97(5)	966.6(9)	0.2340
HSC-60	1.20	0.2024	2.0845	0.2130	0.417	0.056	0.333	0.881	0.083	0	**MG**	7.3488(7)	18.8009(18)	7.3950(7)	91.392(7)	102.185(6)	98.820(7)	985.21(16)	4.40
	25	0	0	0	0	0	0	0	0	0									0.2502
HSC-61	1.20	0.1627	2.1232	0.2141	0.333	0.111	0.333	0.645	0.170	0.067	**AL**	7.3824(16)	18.337(4)	7.3573(16)	93.648(20)	102.452(18)	99.107(18)	955.4(4)	5.94
	25	0	0	0	0	0	0	0	0	0	**MG**	7.3519(14)	18.806(3)	7.4052(14)	91.422(15)	102.188(13)	98.837(13)	987.1(3)	0.2916
HSC-62	1.20	0.1226	2.1623	0.2151	0.250	0.167	0.333	0.455	0.195	0.168	**AL**	7.3813(19)	18.302(5)	7.3374(19)	93.807(21)	102.294(19)	99.119(19)	951.1(4)	4.90
	25	0	0	0	0	0	0	0	0	0	**MG**	7.3418(26)	18.720(6)	7.3919(27)	91.40(3)	102.123(25)	98.738(25)	980.1(6)	0.2631
HSC-63	1.20	0.0822	2.2017	0.2161	0.167	0.222	0.333	0.294	0.256	0.215	**AL**	7.3774(13)	18.273(4)	7.3284(13)	93.811(13)	102.247(12)	99.134(12)	948.0(3)	5.12
	25	0	0	0	0	0	0	0	0	0	**MG**	7.337(4)	18.535(8)	7.396(4)	91.69(5)	101.98(4)	98.48(4)	971.2(9)	0.2716
HSC-64	1.20	0.0413	2.2415	0.2172	0.083	0.278	0.333	0.113	0.215	0.377	**AL**	7.3805(8)	18.2782(22)	7.3271(8)	93.863(8)	102.227(7)	99.116(7)	948.60(18)	3.90
	25	0	0	0	0	0	0	0	0	0	**MG**	7.3122(24)	18.362(4)	7.4238(23)	92.306(27)	101.733(25)	98.070(26)	963.9(5)	0.2423
HSC-65	1.20	0.1558	2.0880	0.2562	0.320	0.053	0.400	0.632	0.055	0.191	**AL**	7.379(4)	18.449(9)	7.353(3)	92.88(4)	102.53(4)	98.86(4)	961.8(8)	5.31
	25	0	0	0	0	0	0	0	0	0	**MG**	7.3486(17)	18.795(4)	7.4041(17)	91.413(18)	102.175(16)	98.844(15)	986.0(4)	0.2767
HSC-66	1.20	0.1174	2.1252	0.2574	0.240	0.107	0.400	0.446	0.081	0.288	**AL**	7.3796(20)	18.299(5)	7.3367(20)	93.818(21)	102.269(20)	99.156(20)	950.6(5)	5.45
	25	0	0	0	0	0	0	0	0	0	**MG**	7.3426(27)	18.716(6)	7.3913(28)	91.39(3)	102.107(26)	98.718(26)	980.0(6)	0.2802
HSC-67	1.20	0.0786	2.1628	0.2586	0.160	0.160	0.400	0.267	0.120	0.368	**AL**	7.3755(13)	18.277(4)	7.3266(13)	93.832(14)	102.213(13)	99.163(12)	947.8(3)	4.67
	25	0	0	0	0	0	0	0	0	0	**MG**	7.338(4)	18.406(8)	7.389(4)	90.96(5)	102.06(4)	97.50(4)	966.6(9)	0.2614
HSC-68	1.20	0.0395	2.2007	0.2598	0.080	0.213	0.400	0.112	0.083	0.509	**AL**	7.3799(8)	18.2665(21)	7.3256(7)	93.863(8)	102.216(7)	99.125(7)	947.73(18)	3.84
	25	0	0	0	0	0	0	0	0	0	**MG**	7.344(4)	18.303(8)	7.393(4)	90.96(6)	101.97(5)	97.16(5)	963.7(9)	0.2380
HSC-69	1.20	0.1098	2.0907	0.2995	0.225	0.050	0.467	0.362	0	0.425	**AL**	7.3755(19)	18.273(5)	7.3327(19)	93.806(20)	102.279(19)	99.138(18)	948.2(4)	5.62
	25	0	0	0	0	0	0	0	0	0	**MG**	7.337(3)	18.691(6)	7.389(3)	91.35(4)	102.083(29)	98.63(3)	977.9(7)	0.2811
HSC-70	1.20	0.0735	2.1257	0.3008	0.150	0.100	0.467	0.264	0.142	0.349	**AL**	7.3741(14)	18.265(4)	7.3264(13)	93.824(14)	102.232(13)	99.182(13)	946.8(3)	5.77
	25	0	0	0	0	0	0	0	0	0	**MG**	7.335(3)	18.357(7)	7.391(4)	91.04(4)	102.03(4)	97.40(4)	964.2(7)	0.2827
HSC-71	1.20	0.0369	2.1609	0.3021	0.075	0.150	0.467	0.092	0	0.606	**AL**	7.3809(7)	18.2606(19)	7.3261(7)	93.855(7)	102.211(7)	99.133(7)	947.62(16)	3.30
	25	0	0	0	0	0	0	0	0	0	**MG**	7.353(5)	18.307(9)	7.392(5)	90.98(6)	101.94(6)	97.32(5)	964.7(10)	0.2228
HSC-72	1.20	0.0652	2.0918	0.3430	0.133	0.044	0.533	0.186	0	0.542	**AL**	7.3766(12)	18.267(3)	7.3258(11)	93.825(12)	102.222(11)	99.154(11)	947.29(27)	4.32
	25	0	0	0	0	0	0	0	0	0	**MG**	7.344(4)	18.391(8)	7.392(5)	91.60(5)	101.82(5)	97.89(5)	966.4(10)	0.2534
HSC-73	1.20	0.0327	2.1230	0.3443	0.067	0.089	0.533	0.073	0	0.618	**AL**	7.3828(7)	18.2585(20)	7.3257(7)	93.858(7)	102.221(7)	99.140(7)	947.64(17)	3.43
	25	0	0	0	0	0	0	0	0	0	**MG**	7.356(7)	18.248(15)	7.397(7)	91.63(10)	101.79(9)	97.45(8)	962.2(16)	0.2216
HSC-74	1.20	0.0245	2.0891	0.3864	0.050	0.033	0.600	0.039	0.054	0.587	**AL**	7.3826(6)	18.2505(16)	7.3262(6)	93.863(6)	102.217(5)	99.151(5)	947.23(13)	3.12
	25	0	0	0	0	0	0	0	0	0	**MG**	7.359(6)	18.316(12)	7.350(6)	90.31(8)	102.54(7)	97.27(7)	958.7(13)	0.2107
HSC-79	1.20	0	2.0950	0	0	0	0	0.007	0	0	**CL**	7.3501(4)	36.3822(18)	7.3325(3)	93.184(3)	102.176(3)	92.458(3)	1910.74(16)	2.57
	75	0	0.2860	0	0	1.000	0	0	1.005	0									0.1856
HSC-80	1.20	0.0245	2.1021	0	0.100	0	0	0.123	0	0	**CL**	7.3507(4)	36.3852(22)	7.3359(4)	93.194(3)	102.173(4)	92.468(4)	1911.93(20)	2.38
	75	0	0.2574	0	0	0.900	0	0	0.882	0									0.1782
HSC-81	1.20	0.0490	2.1092	0	0.200	0	0	0.238	0	0	**CL**	7.34988(29)	36.3598(15)	7.33443(29)	93.1966(26)	102.1406(29)	92.4635(28)	1910.23(14)	2.46
	75	0	0.2288	0	0	0.800	0	0	0.775	0									0.1811
HSC-82	1.20	0.0735	2.1163	0	0.300	0	0	0.358	0	0	**CL**	7.3477(3)	36.3483(17)	7.3336(3)	93.1909(28)	102.144(3)	92.482(3)	1908.80(15)	2.14
	75	0	0.2002	0	0	0.700	0	0	0.659	0									0.1709
HSC-83	1.20	0.0980	2.1234	0	0.400	0	0	0.730	0.015	0	**MG**	7.3495(21)	18.802(6)	7.3981(21)	91.417(22)	102.123(18)	98.784(20)	986.1(5)	15.00
	75	0	0.1716	0	0	0.600	0	0	0.247	0									0.4347

		amount of sulfates weighed out (g)				expected stoichiometry at the *A* site				measured stoichiometry at the A site				lattice parameters (Å, º) and unit cell volume (Å^3) for one or two phases in the sample, as applicable							
sample	water (mL) T (ºC)	Mg Ni	Fe^{3+} Zn	Al Fe^{2+}		Mg Ni	Fe^{3+} Zn	Al Fe^{2+}		Mg Ni	Fe^{3+} Zn	Al Fe^{2+}		type	*a*	*b*	*c*	α	β	γ	*V*	χ^2 wRp
HSC-84	1.20	0.1225	2.1305	0		0.500	0	0		0.817	0	0		**MG**	7.3548(13)	18.801(4)	7.3979(13)	91.361(14)	102.183(12)	98.820(12)	986.4(3)	14.33
	75	0	0.1430	0		0	0.500	0		0	0.203	0										0.4424
HSC-85	1.20	0.1470	2.1376	0		0.600	0	0		0.861	0	0		**MG**	7.3520(8)	18.8060(21)	7.3965(8)	91.364(9)	102.178(7)	98.808(8)	986.18(19)	5.08
	75	0	0.1144	0		0	0.400	0		0	0.141	0										0.2663
HSC-86	1.20	0.1715	2.1447	0		0.700	0	0		0.912	0	0		**MG**	7.3504(7)	18.8059(20)	7.3957(7)	91.356(8)	102.159(7)	98.799(7)	985.96(18)	4.74
	75	0	0.0858	0		0	0.300	0		0	0.100	0										0.2599
HSC-87	1.20	0.1960	2.1518	0		0.800	0	0		0.963	0	0		**MG**	7.3512(7)	18.8036(19)	7.3956(7)	91.348(8)	102.181(7)	98.815(7)	985.81(17)	4.63
	75	0	0.0572	0		0	0.200	0		0	0.044	0										0.2554
HSC-88	1.20	0.2205	2.1589	0		0.900	0	0		0.983	0	0		**MG**	7.3509(14)	18.798(4)	7.3962(14)	91.349(15)	102.177(12)	98.818(13)	985.6(3)	10.28
	75	0	0.0286	0		0	0.100	0		0	0.023	0										0.3700
HSC-89	1.20	0.2450	2.1660	0		0	0	0		1.000	0	0		**MG**	7.3518(14)	18.793(4)	7.3965(14)	91.350(15)	102.191(12)	98.813(13)	985.4(3)	16.52
	75	0	0	0		0	1.000	0		0	0	0										0.4802
HSC-90	1.20	0.4779	2.0221	0		1.000	0	0		not analyzed				**MG**	7.345(3)	18.786(7)	7.389(3)	91.41(3)	102.15(3)	98.80(3)	983.4(7)	6.80
	110	0	0	0		0	0	0														0.3632
HSC-94	1.20	0	2.0709	0.4291		1.000	0	0.445		not analyzed				**AL**	7.390(4)	18.302(12)	7.324(4)	93.91(5)	102.26(4)	98.93(5)	951.1(9)	1.04
	110	0	0	0		0	0	0														0.0786
HSC-95	1.20	0	1.9597	0		0	0	0		0	0.134	0		**MG**	7.359(18)	18.69(5)	7.417(15)	91.03(14)	102.25(14)	98.19(15)	985.4(41)	5.22
	25	0	0.5403	0		0	1.000	0		0	0.799	0										0.2065
HSC-96	1.20	0	1.9696	0		0	0	0		0	0.122	0		**MG**	7.411(19)	18.63(6)	7.467(17)	92.30(14)	102.47(13)	96.72(16)	997.7(46)	8.19
	25	0.5304	0	0		1.000	0	0		0.817	0	0										0.4038
HSC-97	1.20	0	1.9738	0		0	0	0		0	0.014	0		**AL**	7.3869(10)	18.5914(27)	7.3586(10)	92.286(10)	102.283(9)	98.282(10)	974.54(23)	4.01
	25	0	0	0.5262		0	0	1.000		0	0	0.980										0.2446
HSC-99	1.20	0.4289	2.0168	0		0.900	0	0		0.975	0	0		**MG**	7.3471(5)	18.7918(13)	7.3896(5)	91.365(6)	102.167(5)	98.829(5)	983.85(12)	2.51
	25	0.0543	0	0		0.100	0	0		0.049	0	0										0.2308
HSC-100	1.20	0.3803	2.0114	0		0.800	0	0		0.937	0	0		**MG**	7.3450(5)	18.7880(14)	7.3896(5)	91.363(6)	102.165(5)	98.839(5)	983.35(13)	2.78
	25	0.1083	0	0		0.200	0	0		0.076	0	0										0.2411
HSC-101	1.20	0.3319	2.0061	0		0.700	0	0		0.864	0	0		**MG**	7.3462(5)	18.7837(13)	7.3891(5)	91.374(6)	102.165(5)	98.838(5)	983.20(12)	2.61
	25	0.1621	0	0		0.300	0	0		0.136	0	0										0.2320
HSC-102	1.20	0.2837	2.0008	0		0.600	0	0		0.761	0	0		**MG**	7.3453(5)	18.7787(14)	7.3876(5)	91.378(6)	102.156(5)	98.841(5)	982.66(12)	2.66
	25	0.2155	0	0		0.400	0	0		0.239	0	0										0.2357
HSC-103	1.20	0.2358	1.9955	0		0.500	0	0		0.787	0	0		**MG**	7.3456(6)	18.7765(15)	7.3877(6)	91.385(6)	102.165(5)	98.848(6)	982.52(14)	2.86
	25	0.2687	0	0		0.500	0	0		0.238	0	0										0.2421
HSC-104	1.20	0.1881	1.9903	0		0.400	0	0		0.665	0	0		**MG**	7.3467(6)	18.7727(15)	7.3875(6)	91.382(7)	102.166(6)	98.845(6)	982.45(14)	2.75
	25	0.3216	0	0		0.600	0	0		0.351	0	0										0.2373
HSC-105	1.20	0.1407	1.9851	0		0.300	0	0		0.547	0.008	0		**MG**	7.3456(6)	18.7633(15)	7.3875(6)	91.401(7)	102.160(5)	98.852(6)	981.80(14)	2.57
	25	0.3742	0	0		0.700	0	0		0.441	0	0										0.2332
HSC-106	1.20	0.0936	1.9799	0		0.200	0	0		0.319	0	0		**MG**	7.3447(7)	18.7400(18)	7.3838(7)	91.405(8)	102.138(7)	98.881(7)	979.96(16)	3.06
	25	0.4265	0	0		0.800	0	0		0.681	0	0										0.2497
HSC-107	1.20	0.0467	1.9747	0		0.100	0	0		0.182	0	0		**MG**	7.3465(7)	18.7282(20)	7.3842(8)	91.438(9)	102.143(7)	98.878(7)	979.59(18)	3.55
	25	0.4786	0	0		0.900	0	0		0.818	0	0										0.2678
HSC-108	1.20	0.4287	2.0157	0		0.900	0	0		0.944	0.010	0		**MG**	7.3459(5)	18.7925(12)	7.3886(5)	91.365(5)	102.160(4)	98.824(5)	983.63(11)	2.91
	25	0	0.0556	0		0	0.100	0		0	0.040	0										0.2473

	amount of sulfates weighed out (g)				expected stoichiometry at the *A* site			measured stoichiometry at the A site				lattice parameters (Å, º) and unit cell volume (Å^3) for one or two phases in the sample, as applicable							
sample	water (mL) T (ºC)	Mg Ni	Fe^{3+} Zn	Al Fe^{2+}	Mg Ni	Fe^{3+} Zn	Al Fe^{2+}	Mg Ni	Fe^{3+} Zn	Al Fe^{2+}	type	*a*	*b*	*c*	α	β	γ	*V*	χ^2 wRp
HSC-109	1.20	0.3799	2.0093	0	0.800	0	0	0.910	0	0	**MG**	7.3452(5)	18.7924(12)	7.3886(5)	91.383(5)	102.157(4)	98.828(5)	983.52(11)	2.81
	25	0	0.1108	0	0	0.200	0	0	0.090	0									0.2449
HSC-110	1.20	0.3313	2.0030	0	0.700	0	0	0.872	0.008	0	**MG**	7.3463(5)	18.7924(13)	7.3898(5)	91.380(6)	102.164(5)	98.838(5)	983.77(12)	2.43
	25	0	0.1657	0	0	0.300	0	0	0.116	0									0.2266
HSC-111	1.20	0.2831	1.9967	0	0.600	0	0	0.856	0	0	**MG**	7.3472(6)	18.7950(15)	7.3898(6)	91.384(6)	102.169(5)	98.835(5)	984.01(13)	2.27
	25	0	0.2202	0	0	0.400	0	0	0.151	0									0.2205
HSC-112	1.20	0.2352	1.9904	0	0.500	0	0	0.783	0.018	0	**MG**	7.3445(5)	18.7905(12)	7.3878(5)	91.381(5)	102.166(4)	98.834(5)	983.17(11)	2.77
	25	0	0.2744	0	0	0.500	0	0	0.189	0									0.2403
HSC-113	1.20	0.1876	1.9842	0	0.400	0	0	0.690	0.014	0	**MG**	7.3454(5)	18.7917(13)	7.3874(5)	91.384(6)	102.153(5)	98.849(5)	983.29(12)	3.72
	25	0	0.3282	0	0	0.600	0	0	0.289	0									0.2472
HSC-114	1.20	0.1402	1.9780	0	0.300	0	0	0.613	0.003	0	**MG**	7.3465(5)	18.7924(14)	7.3881(5)	91.396(6)	102.154(5)	98.844(5)	983.57(13)	3.41
	25	0	0.3818	0	0	0.700	0	0	0.383	0									0.2391
HSC-115	1.20	0.0932	1.9719	0	0.200	0	0	0.483	0.005	0	**MG**	7.3464(6)	18.7893(17)	7.3878(6)	91.408(7)	102.158(6)	98.851(6)	983.31(15)	3.19
	25	0	0.4349	0	0	0.800	0	0	0.509	0									0.2305
HSC-116	1.20	0.0465	1.9658	0	0.100	0	0	0.265	0	0	**MG**	7.3491(7)	18.7874(20)	7.3891(7)	91.419(8)	102.167(7)	98.869(7)	983.64(18)	3.42
	25	0	0.4878	0	0	0.900	0	0	0.735	0									0.2368
HSC-128	1.20	0	1.9738	0	0	0	0	0	0.002	0	**AL**	7.3858(9)	18.5917(25)	7.3543(8)	92.273(9)	102.274(8)	98.290(9)	973.87(21)	6.56
	25	0	0	0.5262	0	0	1.000	0	0	0.997									0.3105
HSC-129	1.20	0.4290	2.0172	0	0.900	0	0	0.915	0.022	0	**MG**	7.3465(6)	18.7979(14)	7.3903(6)	91.368(6)	102.174(5)	98.827(5)	984.15(13)	6.42
	25	0	0	0.0538	0	0	0.100	0	0	0.053									0.2993
HSC-130	1.20	0.3804	2.0123	0	0.800	0	0	0.895	0.007	0	**MG**	7.3460(5)	18.7970(13)	7.3893(5)	91.362(6)	102.179(4)	98.830(5)	983.88(12)	5.21
	25	0	0	0.1073	0	0	0.200	0	0	0.094									0.2740
HSC-131	1.20	0.3321	2.0074	0	0.700	0	0	0.824	0.038	0	**MG**	7.3457(6)	18.7986(16)	7.3882(6)	91.371(7)	102.173(5)	98.826(6)	983.81(14)	6.92
	25	0	0	0.1605	0	0	0.300	0	0	0.119									0.3140
HSC-132	1.20	0.2839	2.0025	0	0.600	0	0	0.816	0.034	0	**MG**	7.3455(6)	18.7989(14)	7.3886(6)	91.371(6)	102.175(5)	98.827(5)	983.83(13)	4.07
	25	0	0	0.2135	0	0	0.400	0	0	0.133									0.2389
HSC-133	1.20	0.2360	1.9977	0	0.500	0	0	0.722	0.052	0	**MG**	7.3453(5)	18.8021(13)	7.3889(5)	91.366(6)	102.169(5)	98.834(5)	984.03(12)	4.92
	25	0	0	0.2663	0	0	0.500	0	0	0.200									0.2653
HSC-134	1.20	0.1884	1.9929	0	0.400	0	0	0.639	0.051	0	**MG**	7.3463(7)	18.8057(18)	7.3892(7)	91.371(8)	102.176(6)	98.831(7)	984.36(17)	6.28
	25	0	0	0.3187	0	0	0.600	0	0	0.285									0.2974
HSC-135	1.20	0.1409	1.9881	0	0.300	0	0	0.496	0.074	0	**MG**	7.3504(9)	18.8162(24)	7.3934(9)	91.390(10)	102.179(8)	98.813(9)	986.04(22)	6.48
	25	0	0	0.3710	0	0	0.700	0	0	0.392									0.3023
HSC-136	1.20	0.0937	1.9833	0	0.200	0	0	0.355	0.087	0	**MG**	7.3563(13)	18.820(3)	7.3977(13)	91.430(14)	102.225(12)	98.780(12)	987.5(3)	5.96
	25	0	0	0.4229	0	0	0.800	0	0	0.514									0.2972
HSC-137	1.20	0.0468	1.9786	0	0.100	0	0	0.185	0.097	0	**MG**	7.3604(25)	18.779(6)	7.4062(26)	1.468(27)	102.252(23)	98.416(24)	987.9(6)	10.63
	25	0	0	0.4747	0	0	0.900	0	0	0.670									0.3963
HSC-138	1.20	0	1.9831	0.0411	0	0	0.067	0	0	0.023	**AL**	7.3870(10)	18.5740(27)	7.3537(10)	92.276(10)	102.261(9)	98.279(10)	973.09(23)	4.98
	25	0	0	0.4758	0	0	0.900	0	0	0.966									0.2790
HSC-141	1.20	0	2.0115	0.1667	0	0	0.267	0	0.097	0.306	**AL**	7.3813(10)	18.2282(28)	7.3260(10)	93.769(10)	102.243(9)	98.959(9)	946.53(23)	5.36
	25	0	0	0.3217	0	0	0.600	0	0	0.395									0.2764
HSC-142	1.20	0	2.0212	0.2094	0	0	0.333	0	0.110	0.388	**AL**	7.3848(8)	18.2325(22)	7.3259(8)	93.821(8)	102.238(7)	99.053(7)	946.84(18)	5.48
	25	0	0	0.2694	0	0	0.500	0	0	0.253									0.2788

sample	water (mL) T (ºC)	amount of sulfates weighed out (g) Mg Ni	Fe^{3+} Zn	Al Fe^{2+}	expected stoichiometry at the *A* site Mg Ni	Fe^{3+} Zn	Al Fe^{2+}	measured stoichiometry at the A site Mg Ni	Fe^{3+} Zn	Al Fe^{2+}	type	lattice parameters (Å, º) and unit cell volume (Å^3) for one or two phases in the sample, as applicable *a*	*b*	*c*	α	β	γ	*V*	χ^2 wRp
HSC-143	1.20	0	2.0309	0.2525	0	0	0.400	0	0.115	0.435	**AL**	7.3842(7)	18.2368(20)	7.3260(7)	93.842(8)	102.231(7)	99.090(7)	946.87(17)	5.44
	25	0	0	0.2165	0	0	0.400	0	0	0.176									0.2772
HSC-144	1.20	0	2.0408	0.2960	0	0	0.467	0	0.098	0.475	**AL**	7.3840(7)	18.2395(18)	7.3253(6)	93.850(7)	102.217(6)	99.107(6)	946.88(15)	4.15
	25	0	0	0.1632	0	0	0.300	0	0	0.141									0.2428
HSC-145	1.20	0	2.0507	0.3400	0	0	0.533	0	0.111	0.501	**AL**	7.3830(6)	18.2420(17)	7.3257(6)	93.870(6)	102.216(6)	99.141(6)	946.79(14)	3.81
	25	0	0	0.1093	0	0	0.200	0	0	0.083									0.2324
HSC-146	1.20	0	2.0607	0.3843	0	0	0.600	0	0.086	0.554	**AL**	7.3830(6)	18.2444(15)	7.3253(5)	93.881(6)	102.208(5)	99.155(5)	946.85(13)	3.11
	25	0	0	0.0549	0	0	0.100	0	0	0.040									0.2115
HSC-147	1.17	0.2450	2.166	0	1.000	0	0	1.047	0	0	**MG**	7.3468(5)	18.7940(10)	7.3874(5)	91.365(6)	102.184(5)	98.820(5)	983.60(10)	1.59
	75	0	0	0	0	0	0	0	0	0									0.1163
HSC-148	1.17	0	2.500	0	0	0.667	0	0	0.667	0	**AL**	7.3873(2)	18.365(1)	7.3280(2)	93.963(2)	102.202(2)	98.939(2)	954.10(10)	1.88
	75	0	0	0	0	0	0	0	0	0									0.1703
HSC-149	1.17	0	2.177	0.224	0	0	0.667	0	0.100	0.567	**AL**	7.3838(4)	18.2490(10)	7.3243(4)	93.902(4)	102.198(4)	99.171(4)	947.00(10)	2.73
	75	0	0	0	0	0	0	0	0	0									0.2012
HSC-150	1.17	0	2.098	0	0	0	0	0	0.394	0	**AL**	7.3953(7)	18.3140(20)	7.3287(7)	93.499(8)	102.244(7)	98.924(7)	953.70(20)	3.70
	75		$CuSO_4$ $5H_2O$: 0.249 g			Cu: 1.000			Cu: 0.401										0.2156
HSC-151	1.17	0	2.106	0	0	0	0	not analyzed			**CL**	7.3504(3)	36.3110(20)	7.3354(3)	93.187(3)	102.152(3)	92.498(3)	1907.90(10)	2.37
	75	0.2630	0	0	1.000	0	0												0.1719
MAC-1	1.17	0	2.177	0.224	0	0	0.667	0	0.002	0.665	**AL**	7.3842(4)	18.2330(10)	7.3249(3)	93.888(4)	102.215(3)	99.197(4)	946.20(10)	1.64
	75	0	0	0	0	0	0	0	0	0									0.2581
MAC-2	1.17	0.0245	2.1759	0.2016	0.100	0	0.600	0.015	0.137	0.519	**AL**	7.3830(4)	18.2320(10)	7.3226(4)	93.895(4)	102.205(4)	99.189(4)	945.80(10)	1.68
	75	0	0	0	0	0	0	0	0	0									0.2642
MAC-3	1.17	0.0490	2.1748	0.1792	0.200	0	0.533	0.020	0.149	0.505	**AL**	7.3846(4)	18.2360(10)	7.3242(4)	93.895(4)	102.210(4)	99.189(4)	946.30(10)	1.37
	75	0	0	0	0	0	0	0	0	0									0.2440
MAC-4	1.17	0.0735	2.1737	0.1568	0.300	0	0.467	0.127	0.134	0.448	**AL**	7.3833(4)	18.2370(10)	7.3244(4)	93.895(4)	102.208(4)	99.174(4)	946.30(10)	1.19
	75	0	0	0	0	0	0	0	0	0	**MG**	7.340(4)	18.772(6)	7.392(4)	91.41(5)	102.10(4)	98.77(4)	982.5(8)	0.2256
MAC-5	1.17	0.0980	2.1726	0.1344	0.400	0	0.400	0.405	0.104	0.292	**AL**	7.3817(7)	18.2420(20)	7.3281(7)	93.900(8)	102.226(7)	99.190(7)	946.70(20)	1.36
	75	0	0	0	0	0	0	0	0	0	**MG**	7.3446(10)	18.7930(20)	7.3891(10)	91.360(12)	102.131(10)	98.833(10)	983.70(20)	0.2374
MAC-6	1.17	0.1225	2.1715	0.1120	0.500	0	0.333	0.604	0.071	0.193	**MG**	7.3450(7)	18.8050(20)	7.3906(7)	91.378(9)	102.155(7)	98.816(7)	984.50(20)	1.55
	75	0	0	0	0	0	0	0	0	0	**AL**	7.3839(12)	18.248(3)	7.3334(11)	93.925(13)	102.230(12)	99.175(12)	948.0(3)	0.2501
MAC-7	1.17	0.1470	2.1704	0.0896	0.600	0	0.267	0.971	0	0.020	**MG**	7.3469(4)	18.8060(10)	7.3904(4)	91.364(5)	102.166(4)	98.809(4)	984.70(10)	1.54
	75	0	0	0	0	0	0	0	0	0									0.2536
MAC-8	1.17	0.1715	2.1693	0.0672	0.700	0	0.200	0.969	0	0.024	**MG**	7.3492(5)	18.8060(10)	7.3918(5)	91.357(5)	102.164(4)	98.817(5)	985.20(10)	1.42
	75	0	0	0	0	0	0	0	0	0									0.2427
MAC-9	1.17	0.1960	2.1682	0.0448	0.800	0	0.133	0.983	0	0.011	**MG**	7.3481(7)	18.7970(20)	7.3917(7)	91.368(8)	102.172(7)	98.825(7)	984.50(20)	2.99
	75	0	0	0	0	0	0	0	0	0									0.3399
MAC-10	1.17	0.2205	2.1671	0.0224	0.900	0	0.067	1.000	0	0	**MG**	7.3473(7)	18.7990(20)	7.3928(7)	91.373(8)	102.173(7)	98.816(7)	984.70(20)	2.61
	75	0	0	0	0	0	0	0	0	0									0.3182
MAC-11	1.17	0.2450	2.1660	0	1.000	0	0	1.000	0	0	**MG**	7.3495(6)	18.8070(20)	7.3933(6)	91.373(7)	102.169(6)	98.810(6)	985.50(20)	1.85
	75	0	0	0	0	0	0	0	0	0									0.2728
FAC-1	1.17	0	2.2093	0.2016	0	0.067	0.600	0	0.076	0.590	**AL**	7.3821(5)	18.2250(20)	7.3235(5)	93.894(5)	102.214(5)	99.203(5)	945.30(10)	6.19
	75	0	0	0	0	0	0	0	0	0									0.3031

		amount of sulfates weighed out (g)				expected stoichiometry at the *A* site				measured stoichiometry at the A site				lattice parameters (Å, º) and unit cell volume (Å^3) for one or two phases in the sample, as applicable							
sample	water (mL) T (ºC)	Mg Ni	Fe^{3+} Zn	Al Fe^{2+}		Mg Ni	Fe^{3+} Zn	Al Fe^{2+}		Mg Ni	Fe^{3+} Zn	Al Fe^{2+}	type	*a*	*b*	*c*	α	β	γ	*V*	χ^2 wRp
FAC-2	1.17 75	0 0	2.2416 0	0.1792 0		0 0	0.133 0	0.533 0		0 0	0.076 0	0.590 0	**AL**	7.3819(9)	18.233(3)	7.3221(9)	93.896(9)	102.208(8)	99.188(9)	945.60(20)	7.62 0.3469
FAC-3	1.17 75	0 0	2.2739 0	0.1568 0		0 0	0.200 0	0.467 0		0 0	0.111 0	0.556 0	**AL**	7.3843(5)	18.2290(20)	7.3258(5)	93.900(5)	102.212(5)	99.195(5)	946.10(10)	6.37 0.3020
FAC-4	1.17 75	0 0	2.3062 0	0.1344 0		0 0	0.267 0	0.400 0		0 0	0.139 0	0.528 0	**AL**	7.3847(7)	18.2350(20)	7.3246(7)	93.892(7)	102.210(7)	99.188(7)	946.30(20)	8.20 0.3478
FAC-5	1.17 75	0 0	2.3385 0	0.1120 0		0 0	0.333 0	0.333 0		0 0	0.163 0	0.504 0	**AL**	7.3847(8)	18.2380(20)	7.3242(8)	93.895(8)	102.213(7)	99.178(7)	946.40(20)	9.27 0.3726
FAC-6	1.17 75	0 0	2.3708 0	0.0896 0		0 0	0.400 0	0.267 0		0 0	0.223 0	0.444 0	**AL**	7.3837(6)	18.2470(20)	7.3230(6)	93.905(6)	102.209(5)	99.159(6)	946.70(20)	8.96 0.3531
FAC-7	1.17 75	0 0	2.4031 0	0.0672 0		0 0	0.467 0	0.200 0		0 0	0.313 0	0.353 0	**AL**	7.3857(7)	18.2640(20)	7.3250(7)	93.910(7)	102.214(6)	99.133(7)	948.20(20)	5.66 0.2947
FAC-8	1.17 75	0 0	2.4354 0	0.0448 0		0 0	0.533 0	0.133 0		0 0	0.392 0	0.274 0	**AL**	7.3846(6)	18.2730(20)	7.3238(6)	93.933(6)	102.201(6)	99.094(6)	948.50(20)	5.25 0.2773
FAC-9	1.17 75	0 0	2.4677 0	0.0224 0		0 0	0.600 0	0.067 0		0 0	0.523 0	0.144 0	**AL**	7.3868(6)	18.3130(20)	7.3264(6)	93.948(6)	102.211(5)	99.011(5)	951.40(10)	5.60 0.2847
FAC-10	1.17 75	0 0	2.500 0	0 0		0 0	0.667 0	0 0		0 0	0.667 0	0 0	**AL**	7.3873(2)	18.3560(10)	7.3280(2)	93.963(2)	102.202(2)	98.939(2)	954.1(1)	2.73 0.2012